

Politecnico di Torino

Master's Degree in Energy and Nuclear Engineering A.a. 2024/2025

Development of a Multi-Objective Techno-environomic Optimisation Framework

Design of Floating Platforms and Mooring Lines

Supervisors:

Author:

Giuseppe Giorgi Markel Peñalba Retes Bruno Paduano Francesca Colombi

Abstract

The growing global demand for renewable energy is accelerating the development of offshore wind technology, with floating offshore wind turbines (FOWTs) emerging as a key option to harness wind resources in deeper waters. This technology has great potential but is still at an early stage, where high costs, technical complexity, and design uncertainties remain major barriers to large-scale deployment. To make FOWTs a feasible option, optimisation is essential to reduce costs and improve performance, while a multidisciplinary approach is required to properly account for the coupled nature and complexity of the system.

Within the INF4INITY project, this thesis develops a multi-objective optimisation methodology for the GICON-SOF Tension-Leg Platform supporting the IEA 15-MW reference wind turbine. The approach explores alternative platform configurations by varying the main external dimensions of the substructure, which directly affect structural mass, hydrostatic stiffness, and hydrodynamic response. In parallel, the optimisation also accounts for the sizing of the mooring lines, whose dimensions and loads are strongly coupled with the platform geometry. The optimisation is implemented using the NSGA-II genetic algorithm, chosen for its ability to explore large design spaces while converging towards Pareto-optimal solutions. The workflow integrates parametric geometry generation in SALOME, hydrodynamic analysis in NEMOH, and simplified techno-economic and environmental models.

The optimisation framework addresses three objectives: hydrodynamic response, an economic indicator and an environmental indicator. The design space is explored under stability and feasibility constraints, imposed respectively on platform motions and mooring system characteristics. Preliminary simulations show that cost and emissions are both dominated by steel mass. Refining the cost and emission functions to capture additional contributions will help decouple these objectives and offer a more realistic view of design trade-offs.

The methodology developed in this thesis provides a functional baseline tool that integrates technical, economic, and environmental objectives, and is ready to be expanded with additional factors such as anchoring systems, installation activities, and end-of-life operations. As part of the INF⁴INiTY project, this work represents an initial step towards more comprehensive optimisation approaches for floating wind platforms.

Contents

1	Intro	oduction	n	10
2	Lite	rature I	Review	13
	2.1	Offsho	re Wind Turbines	13
		2.1.1	Floating Offshore Wind Turbines (FOWT)	15
		Ser	mi-submersible platforms	17
		Ter	nsion-Leg Platforms (TLPs)	18
	2.2	Optim	ization methods	19
		2.2.1	Optimization approaches and methodologies	20
		2.2.2	Genetic Algorithms (GA)	22
3	Met	hodolog	\mathbf{y}	24
	3.1	Workfl	ow Overview	24
	3.2	Optim	isation algorithm (NSGA-II)	25
		Ini	tialization	26
		Par	rent Selection	27
		Off	spring Creation	27
		En	vironmental Selection	28
		Ter	rmination Criteria	29
	3.3	Optim	ization objectives	29
		3.3.1	Technical objective	30
		3.3.2	Economic objective	33
		3.3.3	Environmental objective	35
	3.4	Metoc	ean conditions	36
		Wa	ve conditions	36
	3.5	Evalua	ation function	38
		3.5.1	Geometry generation and hydrostatics (SALOME)	39
		3.5.2	Hydrodynamic analysis (NEMOH)	40
		3.5.3	Constraints	41
		Res	sonance constraint	42
		Mo	orings constraint	43
		3.5.4	Objective evaluation	46

		RAO-based Motion Metric	46
		COP-based Cost Metric	47
		Emissions Metric	49
4	Inpu	at Data & Case Study	50
	4.1	Geometry	50
	4.2	Wind Turbine	53
	4.3	Environmental conditions	56
	4.4	Optimization framework	58
		4.4.1 Genetic algorithm setup	58
		4.4.2 Constraints	58
5	Resu	alts and Discussions	60
5	Resu	Results of techno-economic optimization	60
5			
5	5.1	Results of techno-economic optimization	60
5	5.1 5.2	Results of techno-economic optimization	60 65
5	5.1 5.2	Results of techno-economic optimization	60 65 70
5	5.1 5.2	Results of techno-economic optimization Results of techno-environomic optimization Selected individuals Techno-economic optimisation	60 65 70 71

List of Figures

1.1	New offshore installations (MW) [13]	10
1.2	Published papers on design optimisation (2000–2020) [7]	12
2.1	Growth in offshore wind turbine capacity, rotor diameter, and tip height over time [13].	14
2.2	Fixed and floating substructures and their typical water depth range[1].	15
2.3	Illustrative cost breakdown of a floating offshore wind reference project.	
	Source: [26]	16
2.4	Optimisation algorithms used within the literature [28]	22
3.1	Workflow	24
3.2	NSGA-II algorithm scheme	25
3.3	NSGA-II non dominated sorting	26
3.4	NSGA-II crowding distance	27
3.5	Offshore floating wind turbine platform degrees of freedom [10]	31
3.6	Evaluation function workflow	38
4.1	Original geometry	51
4.2	Panel mesh of the simplified geometry exported from SALOME and used in Nemoh (1574 panels)	52
4.3	Steady-state power curves at different platform pitch stiffnesses	54
4.4	AEP at different platform pitch stiffnesses (related to different maximum static pitch angles)	55
4.5	Steady-state values of rotor speed, blade pitch angle, generator torque,	
	power, thrust, and structure pitch angle at different platform pitch	
	stiffnesses.	55
4.6	Wind speed occurrence distribution	57
4.7	Scatter diagram of sea state occurrences in terms of H_s and T_p	57
4.8	Set of JONSWAP spectra weighted by their relative occurrence	57
4.9	RAOs of the reference configuration compared with the site-specific	
	JONSWAP spectrum.	59
5.1	Population convergence in the techno-economic optimization	60

5.2	Normalised techno-economic Pareto front in the CAPEX–RAO–AEP	
	space with respect to the reference configuration. Values below 1	
	indicate improvement	61
5.3	Two-dimensional projections of the techno-economic Pareto front:	
	(top) AEP–RAO, (middle) AEP–CAPEX, and (bottom) RAO–CAPEX.	
	The colour scale in each panel represents the third objective	62
5.4	Objectives as a function of D_P	63
5.5	Objectives as a function of Draft	63
5.6	Objectives as a function of L_X	63
5.7	Objectives as a function of $L_{Ballast}$	64
5.8	Objectives as a function of mooring line equivalent diameter	64
5.9	Population convergence in the techno-environomic optimization	65
5.10	Normalised techno-environomic Pareto front in the COP–RAO–EOP	
	space with respect to the reference configuration. Values below 1	
	indicate improvement	66
5.11	Two-dimensional projections of the techno-environomic Pareto front:	
	(top) EOP-COP, (middle) EOP-RAO, and (bottom) RAO-COP.	
	The colour scale in each panel represents the third objective	67
5.12	Objectives as a function of D_P	68
5.13	Objectives as a function of Draft	68
5.14	Objectives as a function of L_x	68
5.15	Objectives as a function of $L_{Ballast}$	69
5.16	Objectives as a function of equivalent mooring line diameter	69
5.17	Techno-economic Pareto front with genotype-based selected individ-	
	uals (red) and reference configuration (black)	71
5.18	Radar plots of the selected individuals in the techno-economic opti-	
	misation	72
5.19	Techno-environomic Pareto front with genotype-based selected indi-	
	viduals (red) and reference configuration (black)	74
5.20	Radar plots of the selected individuals in the techno-environomic op-	
	timisation	75

List of Tables

2.1	Overview of optimization algorithms for wind turbine applications,	
	categorized by method, gradient requirements, and multi-objective	
	capability (reproduced from [19])	21
4.1	Optimization variables: reference values and search ranges	53
4.2	Key parameters of the IEA 15-MW reference wind turbine [4]	54
4.3	Main NSGA-II settings.	58
4.4	Constraints considered in the optimization	59
5.1	Selected individuals from the techno-economic optimisation and ref-	
	erence configuration	73
5.2	Selected individuals from the techno-environomic optimisation and	
	reference configuration	76

List of Acronyms

AEP Annual Energy Production

BEM Boundary Element Method

CAPEX Capital Expenditure

COP Cost Over Productivity

DOF Degree of Freedom

EA Elastic Modulus (Axial Stiffness)

EIA Environmental Impact Assessment

EOP Emissions Over Productivity)

GA Genetic Algorithm

GWEC Global Wind Energy Council

IEA International Energy Agency

INF⁴INiTY INtegrated designs for Future Floating oFFshore wINd farm

TechnologY

JONSWAP Joint North Sea Wave Project

LCA Life-Cycle Assessment

LCOE Levelized Cost of Energy

MBL Minimum Breaking Load

MDO Multi-Disciplinary Optimisation

MOEA Multi-Objective Evolutionary Algorithm

MSL Mean Sea Level

NID Nature-Inclusive Design

NSGA-II Non-dominated Sorting Genetic Algorithm II

OPEX Operational Expenditure

RAO Response Amplitude Operator

SDG Sustainable Development Goal

TLP Tension-Leg Platform

TRL Technology Readiness Level

1. Introduction

The global energy mix is progressively shifting towards clean and sustainable sources, with solar and wind power gaining increasing relevance. At the global scale, offshore wind has experienced rapid growth over the last two decades. According to the Global Wind Energy Council (GWEC) [13], 8 GW of new offshore wind capacity was grid-connected worldwide in 2024, bringing total installed capacity to 83.2 GW by the end of the year. The growth in annual offshore additions shown in Figure 1.1 highlights the accelerating pace of deployment, which has increased the share of offshore in global new wind installations from 4% to 7%.

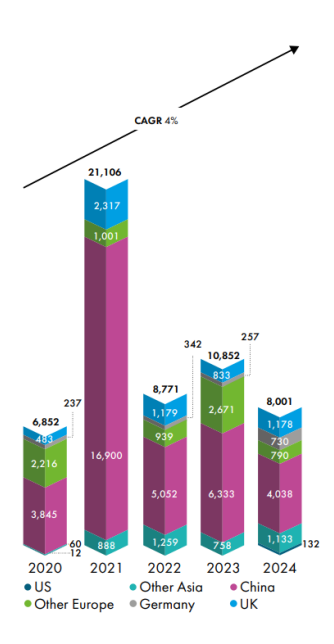


Figure 1.1: New offshore installations (MW) [13]

In the European context, wind energy has consolidated its role as one of the main contributors to renewable electricity generation. The region currently counts about 285 GW of installed capacity, of which 248 GW onshore and 37 GW offshore. With annual installations expected to average 26 GW, a total of 156 GW of offshore wind capacity is projected to be added worldwide between 2025 and 2030 [31]. This expansion has been driven by favorable metocean conditions, continuous technological progress, and strong policy incentives. Until now, most offshore deployment has relied on fixed-bottom turbines, which remain commercially viable in water depths up to about 50 m. Beyond this threshold, costs and installation challenges increase sharply, limiting applicability in deep-water areas where wind resources are stronger

and more consistent. Floating offshore wind turbines (FOWTs) offer a promising solution to unlock this potential.

Different concepts of floating platforms and anchoring systems are currently being developed to harness the abundant wind resources available at deep-water sites. The most widely studied solutions include spar-type floaters with catenary moorings, semi-submersibles that exploit their large waterplane area for stability, tension-leg platforms (TLPs) stabilised by taut tendons, and barge-type platforms [32]. Each configuration offers distinct advantages but also faces specific technical and economic challenges.

The large-scale deployment of floating offshore wind is still constrained by technical and economic barriers. Capital expenditures remain high, with the floating substructure representing the largest cost component, accounting for about 36% of total CAPEX. Additional cost drivers include mooring systems, installation activities, and operation and maintenance requirements[5]. The structural and hydrodynamic behaviour of floating platforms is complex, and the limited operational experience increases uncertainty in performance prediction, slowing down the expected cost reductions. For these reasons, floating wind, despite decades of research and several demonstration projects, is still at a pre-commercial stage. Continued investments in research and innovation are essential to improve technical reliability, reduce costs, and make floating wind competitive within the broader renewable energy mix.

In recent years, optimisation has emerged as a central research driver in this process. Early studies mainly addressed simplified cost models or the stability of reference 5 MW turbines on spar-type platforms. More recently, optimisation frameworks have extended to larger 10–15 MW machines, exploring different platform concepts and design variables, often through multi-objective formulations that seek trade-offs between structural mass, hydrodynamic behaviour, mooring loads, and annual energy production. Genetic algorithms, and in particular NSGA-II, have been widely adopted tools thanks to their ability to explore large design spaces and identify Pareto-optimal solutions across conflicting objectives. The growing attention of the scientific community is reflected in the rapid increase of publications in this field, as shown in Figure 1.2 [7].

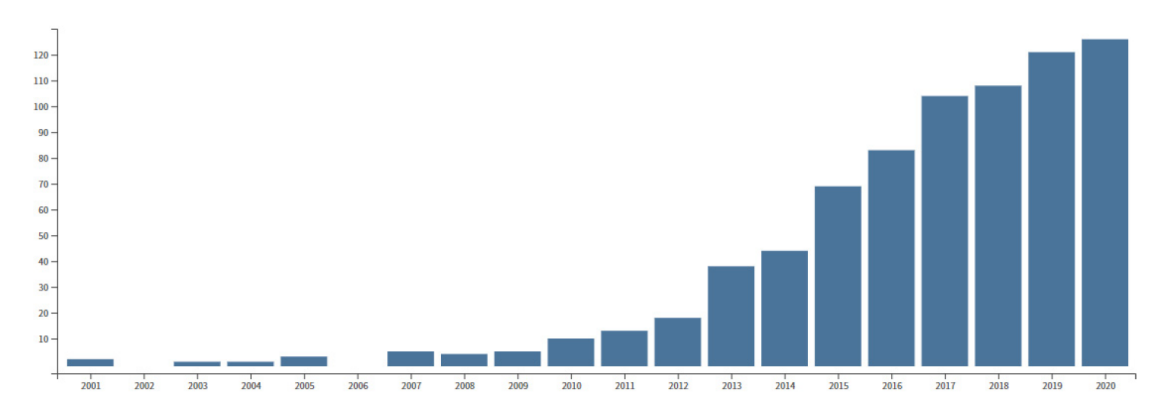


Figure 1.2: Published papers on design optimisation (2000–2020) [7].

Most optimisation studies concentrate on technical and economic performance, while environmental aspects are often assessed separately, typically through post-processing analyses. Life Cycle Assessment (LCA) has been applied in some cases to quantify greenhouse gas emissions, energy payback time, or material use, but such metrics are rarely embedded directly into optimisation frameworks. As a result, the trade-offs relevant for sustainable deployment are not always fully captured. Integrating environmental criteria alongside technical stability and economic viability can therefore represent a valuable step towards more comprehensive and balanced design approaches.

This thesis contributes to such a perspective within the Horizon Europe project INF⁴INiTY, which involves thirteen industrial and academic partners across Europe and focuses on advancing floating offshore wind technology through the integration of novel subsea components and Nature-Inclusive Design (NID) solutions, such as gravity anchor systems with scour protection and artificial reef functionalities. Within this framework, the work presented here develops a metaheuristic optimisation methodology applied to the GICON-SOF TLP, a hybrid concept combining semisubmersible and tension-leg features, supporting the IEA 15 MW reference wind turbine. The methodology explores multiple platform configurations and assesses their technical behaviour through hydrostatics and RAOs, their economic viability through CAPEX, AEP and their environmental performance through embodied CO₂ emissions. By systematically integrating these dimensions, the study contributes to the development of optimisation methodologies that can enhance the reliability, cost-effectiveness, and sustainability of floating wind concepts.

2. Literature Review

2.1 Offshore Wind Turbines

Offshore wind power refers to the process of converting wind energy into electricity through the use of wind turbines installed at sea. This technology takes advantage of the unique characteristics of marine environments, where wind conditions are typically more favorable than on land. The smoother surface of the sea and the relative absence of obstacles lead to stronger, more stable, and less turbulent winds. These consistent wind speeds not only improve the efficiency and energy yield of offshore turbines but also reduce mechanical wear and the risk of failures, thereby enhancing the overall reliability and lifespan of the installations. Furthermore, wind speed offshore shows less variation with height compared to onshore sites, which allows turbines to capture significant energy even at relatively lower hub heights [7].

Beyond these technical benefits, offshore wind power offers important social and environmental advantages. By locating wind farms away from densely populated coastal areas, offshore installations help conserve valuable land resources and reduce conflicts over land use. This is particularly relevant in coastal zones, where space limitations constrain onshore renewable deployment. Additionally, public acceptance of offshore wind projects tends to be higher than that of onshore wind farms, as they generally have less impact on local communities [18].

Despite its numerous advantages, offshore wind technology still faces several challenges. Remote marine locations, while favorable for wind resource exploitation, present significant logistical and operational difficulties. Installing and maintaining turbines in such environments requires specialized vessels, equipment, and highly skilled personnel. The transportation of large turbine components from manufacturing sites to offshore locations is often complex and costly. Moreover, harsh marine conditions can delay construction, increase maintenance requirements, and raise overall project risks and costs. From an environmental standpoint, the development and operation of offshore wind farms can disrupt marine ecosystems. Potential impacts include habitat alteration for fish and seabirds, noise pollution during construction, and changes in local water flow patterns, all of which must be carefully managed to minimize ecological consequences.

Like any modern industrial sector, the success of offshore wind depends strongly on continuous technological innovation. The steady increase in turbine size has been a key driver of higher efficiency and reliability, particularly in the offshore segment where multi-megawatt turbines have become the standard. This trend, summarised in Figure 2.1, shows how rotor diameters and tip heights have grown over the past decades, enabling larger power ratings and more competitive energy generation.

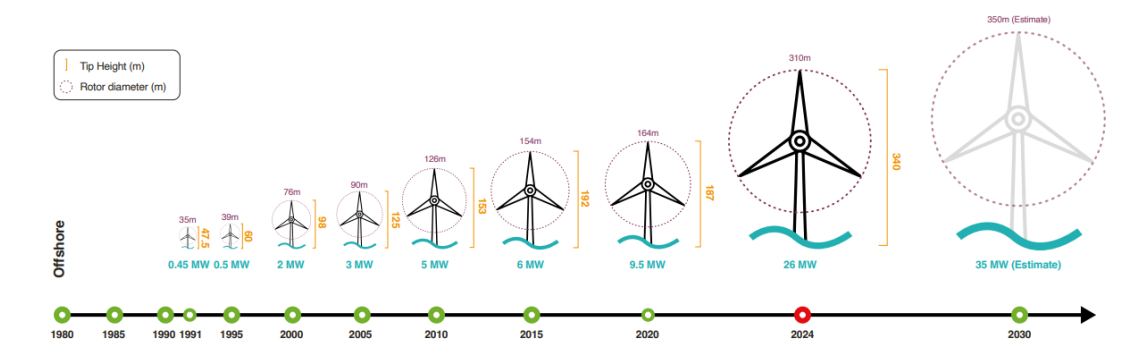


Figure 2.1: Growth in offshore wind turbine capacity, rotor diameter, and tip height over time [13].

Economic viability remains one of the most significant barriers to the future development and investment in offshore wind technology. High capital expenditure, logistical complexity, inflated LCOE and policy volatility all contribute to investment uncertainty and slow the pace of project deployment. Despite these challenges, offshore wind capacity has expanded more than tenfold in the last decade, rising from 7.2 GW in 2013 to 72.7 GW in 2023, with growth driven primarily by China, the UK, and Germany. Nevertheless, it still represents a small share of global renewable energy capacity. Looking ahead, the EU targets 100 GW by 2030 [25].

The global offshore wind sector has so far been dominated by bottom-fixed foundations, with monopiles, jackets, and gravity-based structures installed primarily in water depths up to 60–70 m (Figure 2.2). Monopiles in particular account for nearly 80% of all foundations deployed to date, thanks to their cost-effectiveness and mature supply chains [1]. However, around 80% of the world's technical offshore wind potential lies in waters deeper than 60 m, where fixed-bottom concepts become increasingly uneconomical [13]. For this reason, floating offshore wind has emerged as a critical enabling technology, capable of unlocking vast wind resources in deeper waters.

The following section will provide an overview of floating offshore wind turbines, highlighting their technological principles, development trends, and current challenges.

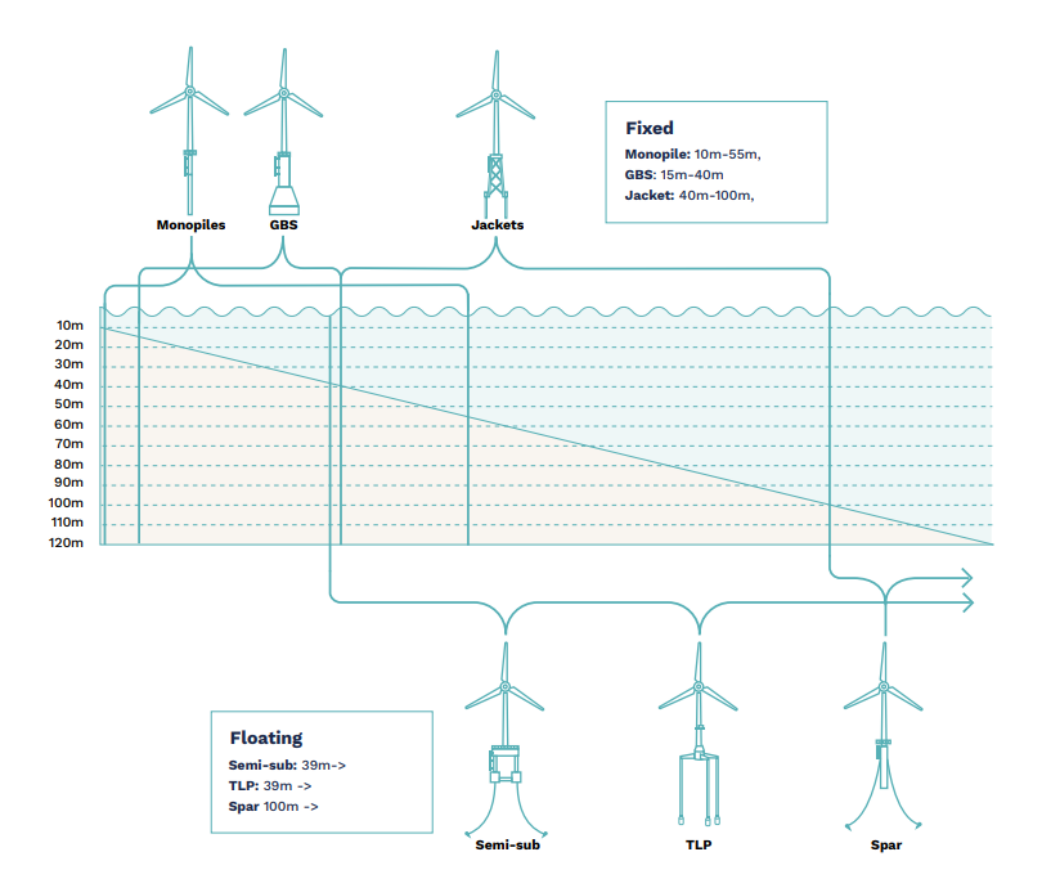


Figure 2.2: Fixed and floating substructures and their typical water depth range[1].

2.1.1 Floating Offshore Wind Turbines (FOWT)

Beyond the opportunities and challenges already discussed for offshore wind, floating technology has emerged as a promising solution to unlock wind resources located in deeper waters. While nearshore sites are becoming saturated, FOWTs enable deployment further offshore, where wind regimes are stronger, less turbulent, and characterised by lower shear, thus generally supporting higher capacity factors. Floating platforms also offer logistical advantages, as turbines can be assembled in sheltered harbours and subsequently towed to site with tugboats, reducing the need for complex offshore lifting operations and mitigating installation risks. From an environmental perspective, the use of mooring and anchoring systems instead of piled foundations can lessen disturbance to marine ecosystems, particularly during installation phases [29].

In addition to the general offshore challenges already noted, floating systems face issues specific to their structural concepts. The greater distance from shore entails longer export cables, which add both costs and transmission losses. Operation and maintenance are further complicated by the motion of floating platforms, the limited availability of weather windows, and the need for specialised vessels.

The economic dimension remains the most critical barrier, explaining why floating wind is still at a pre-commercial stage. Unlike fixed-bottom projects, where the turbine is the main cost driver (about 32% of total CAPEX), in floating systems the substructure dominates, accounting for roughly 36% [5]. To illustrate the magnitude and distribution of costs, Figure 2.3 presents the NREL reference project for a floating substructure, based on empirical cost estimates [26].

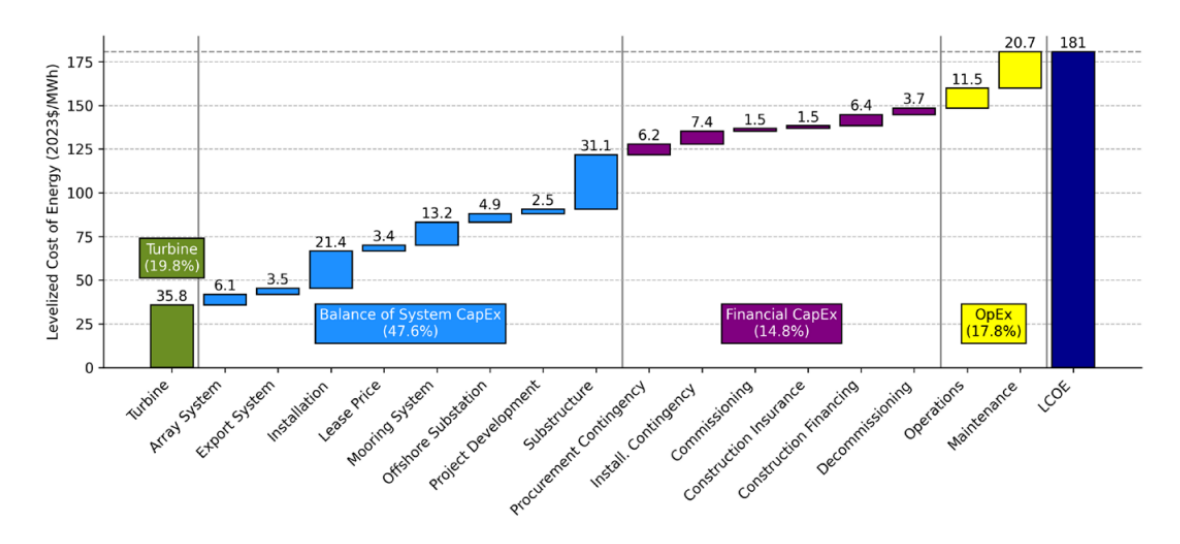


Figure 2.3: Illustrative cost breakdown of a floating offshore wind reference project. Source: [26].

This highlights the need to reduce platform-related expenses to improve competitiveness. In this respect, some cost-reduction pathways have been identified, and expert surveys suggest potential median cost decreases of about 40% by 2050, mainly linked to innovations in foundation design and manufacturing, improved transport and installation strategies, and economies of scale [21]. Although costs remain a central barrier, the benefits of deep-water deployment, such as larger turbines with higher capacity factors, are expected to drive competitiveness, with commercial-scale deployment foreseen within the next decade [13, 21].

The development of floating platforms has drawn on more than six decades of offshore oil and gas experience, where different floater concepts have been applied in harsh marine environments. Floating wind platforms are commonly classified according to their stability mechanism into four main categories [1, 30]:

- Spar-buoys: stability from deep drafts and heavy ballast. Very stable in deep waters but requiring large depths (over 100 m) and challenging transport and installation.
- Semi-submersibles: stability from large waterplane area. Can be deployed at shallower drafts and are easier to tow, but require large amounts of steel, have

complex hydrodynamics, and higher motions in rough seas.

- Barges: wide and shallow hulls providing buoyancy. Simple and relatively inexpensive, with large deck space, but sensitive to waves and suitable mainly for mild environments.
- Tension-leg platforms (TLPs): buoyant hulls restrained by vertical tendons anchored to the seabed. This limits heave and pitch and reduces seabed footprint, but requires costly mooring systems and anchors, specialised installation vessels, and remains at a relatively low technology readiness level.

At present, around 40 floating wind concepts are being tested, prototyped, or developed worldwide, mainly derived from four principal substructure types. Each configuration offers specific advantages and challenges, and no dominant solution has yet emerged, although industry surveys indicate a prevailing preference for semi-submersibles [1]. The present thesis focuses on a case study involving an hybrid designs that combine the stability of TLPs with the constructability and logistical advantages of semi-submersibles.

Semi-submersible platforms

Semi-submersibles are currently the most widely adopted floating wind concept, with several full-scale demonstrators such as WindFloat Atlantic and Kincardine proving their technical feasibility. They achieve stability through a large waterplane area provided by multiple columns connected by pontoons, allowing deployment at moderate water depths with relatively shallow drafts. This configuration facilitates towing and port-side assembly, reducing the need for heavy offshore lifting operations and enabling serial fabrication of modular units [5, 32].

From an economic perspective, however, semi-submersibles are among the most material-intensive solutions, requiring large amounts of steel and complex fabrication processes. This results in high capital expenditure and embodied emissions, making them sensitive to material prices and supply-chain constraints. In terms of environmental performance, life cycle assessments consistently report embodied emissions of about $500{\text -}600~{\rm tCO_2/MW}$ for semi-sub concepts, largely driven by steel production and fabrication processes [20, 24]. Struthers et al. [27] found that manufacturing and materials account for 71–79% of total emissions in floating wind farms around Scotland, confirming that steel production and fabrication processes are the dominant environmental drivers for semi-subs.

Tension-Leg Platforms (TLPs)

Tension-leg platforms (TLPs) design relies on buoyancy exceeding structural weight, which generates an upward restoring force balanced by tensioned vertical mooring lines. This configuration minimises vertical motions and limits pitch and roll, enabling turbines to operate with relatively low dynamic response under demanding metocean conditions. In addition, their compact seabed footprint may facilitate coexistence with other marine activities and reduce the length of inter-array cabling. These technical features suggest potential advantages in terms of material requirements, logistics, and installation. Indeed, several optimisation studies have compared different floater classes and found TLPs to be competitive within the single-body subset. Hall et al. [14] and Karimi et al. [16] showed that TLPs can achieve lower costs while maintaining comparable dynamic performance, positioning them as strong alternatives to spar-buoys and semi-submersibles. For this reason, TLPs are frequently considered a relevant case study in floating offshore wind research.

From an economic perspective, however, these potential benefits are counterbalanced by specific challenges. The high pre-tension in the mooring lines requires anchors capable of resisting large vertical loads, which substantially increases costs. Kausche et al. [17] estimated that the capital expenditure of a floating wind farm based on a TLP design amounts to nearly €18 million for a 6 MW turbine, with the turbine itself contributing about 43% and the TLP structure and moorings around 33%. The resulting levelised cost of energy (LCOE) was approximately 9.5 €c/kWh, comparable with other floating concepts but still above fixed-bottom solutions. Their analysis further showed that fabrication costs, operating expenditures, full load hours, and financing conditions strongly affect economic performance. Under favourable assumptions, serial production and optimised O&M strategies could reduce the LCOE below 7 €c/kWh, improving competitiveness.

In terms of environmental performance, the same study assessed cumulative energy demand and $\rm CO_2$ emissions. Hybrid material solutions combining steel and reinforced concrete achieved significantly lower embodied energy and emissions compared to all-steel variants. Reported values ranged from about 395 t $\rm CO_2/MW$ for concrete—steel hybrids to nearly 690 t $\rm CO_2/MW$ for welded steel structures, largely due to the energy intensity of steel production and welding processes. These results highlight the importance of material selection and fabrication methods for both cost-effectiveness and environmental sustainability.

2.2 Optimization methods

Optimization can be broadly defined as the systematic process of identifying the most advantageous solution among all feasible alternatives that satisfy the constraints of a given problem. In engineering, optimisation is a key tool to support design decisions and address trade-offs among competing criteria. Compared to traditional iterative design approaches, it enables the efficient exploration of large and complex design spaces within reduced computational time, and has been extensively applied in established industrial sectors such as automotive and aerospace [22, 28]. Given the parallels with aerospace engineering and the emerging stage of the floating offshore wind sector, optimisation provides a systematic way to identify, compare, and improve potential support structures.

Optimization problems can generally be formulated as either *single-objective*, where the focus is on maximizing or minimizing a single performance indicator, or *multi-objective*, in which two or more conflicting objectives must be optimized simultaneously. The latter case is particularly relevant for floating offshore wind turbines (FOWTs), where hydrodynamic, aerodynamic, structural, and economic aspects are strongly interdependent, making it necessary to identify a set of trade-off solutions rather than a single optimum. Formally, a multi-objective optimization problem can be stated as:

$$\min_{\mathbf{x} \in \mathcal{X}} \mathbf{F}(\mathbf{x}) = \min_{\mathbf{x} \in \mathcal{X}} \left[f_1(\mathbf{x}), f_2(\mathbf{x}), \dots, f_m(\mathbf{x}) \right]$$

where the feasible design space $\mathcal{X} \subseteq \mathbb{R}^n$ is defined as:

$$\mathcal{X} = \left\{ \mathbf{x} \in \mathbb{R}^n \middle| \begin{cases} \mathbf{x}_{\text{lower}} \le \mathbf{x} \le \mathbf{x}_{\text{upper}}, \\ h_i(\mathbf{x}) = 0, & i = 1, \dots, r, \\ g_j(\mathbf{x}) \ge 0, & j = 1, \dots, s. \end{cases} \right\}$$

with:

- $\mathbf{x} \in \mathbb{R}^n$ the vector of design variables,
- $f_i: \mathbb{R}^n \to \mathbb{R}, i = 1, \dots, m$, the objective functions to be minimized,
- $h_i(\mathbf{x})$ equality constraints,
- $g_j(\mathbf{x})$ inequality constraints,
- \mathbf{x}_{lower} and \mathbf{x}_{upper} bounds on design variables.

Since $\mathbf{F}(\mathbf{x})$ is a vector, when all its components are conflicting no unique solution exists. In such cases, the solution is not a single point but belongs to a Pareto optimal set. A solution $\mathbf{x}^* \in \mathcal{S}$ is defined as Pareto optimal if it is impossible to improve any objective without worsening at least one other, i.e., there is no feasible point $\mathbf{x} \in \mathcal{S}$ such that

$$f_i(\mathbf{x}) \le f_i(\mathbf{x}^*)$$
 for all i ,

with strict inequality for at least one objective. The collection of Pareto optimal solutions forms the Pareto front, representing the best possible trade-offs among conflicting objectives. For two or three objectives, the Pareto front can be visualized as a curve or surface; for higher-dimensional problems, more advanced visualization techniques are required.

In engineering, objectives such as minimising costs, maximising energy output, or reducing environmental impact often conflict. The Pareto front provides a comprehensive view of these trade-offs and serves as a decision-support tool for selecting the most appropriate design.

Different optimisation strategies have been developed to address such problems. Some methods are deterministic and numerical, based on precise mathematical models and exact calculations, while others are heuristic or metaheuristic, which explore the solution space in a more flexible way and are better suited for complex, nonlinear, or multi-modal problems.

2.2.1 Optimization approaches and methodologies

In the context of offshore wind engineering, optimisation problems are particularly challenging due to the strong coupling between hydrodynamic, aerodynamic, structural, and economic aspects, which makes the choice of method critical [7, 28]. A common distinction is between enumerative methods, or *Mathematical Programming* (MP), and heuristic methods, such as *Evolutionary Algorithms* (EA)[12]. MP methods are deterministic and systematic, often able to guarantee convergence to an optimum, but their applicability is limited in nonlinear or high-dimensional problems. Gradient-based techniques such as Sequential Quadratic Programming (SQP) can achieve rapid convergence from a good initial guess, yet remain local methods and are sensitive to the presence of multiple optima.

Heuristic approaches, and in particular Evolutionary Algorithms, provide an alternative for problems where deterministic methods are impractical. EAs are population-based, gradient-free, and treat the optimization process as a "black box," making

them suitable for multi-modal and complex design spaces. They evolve candidate solutions through selection, crossover, and mutation, balancing exploitation of promising designs with broad exploration. Among these, Genetic Algorithms (GA) are the most established. Multi-objective variants such as NSGA-II, SPEA, and PAES are now established standards in engineering design.

Table 2.1 summarises the main optimisation methods currently under study in wind turbine research, highlighting representative algorithms, their gradient requirements, and suitability for multi-objective problems [19].

Table 2.1: Overview of optimization algorithms for wind turbine applications, categorized by method, gradient requirements, and multi-objective capability (reproduced from [19]).

Category	Optimizer	Meaning	Gradient-	MO
	Newton-CG	Newton Conjugate Gradient	based	
	TNC	Truncated Newton	based	
Quasi-Newton method	Powell		based	
	BFGS	Broyden-Fletcher-Goldfarb-Shanno	based	
	L-BFGS-B	Limited-memory BFGS with Box constraints	based	
	FSQP	Feasible SQP	based	
SQP	PSQP	Preconditioned SQP	based	
	SLSQP	Sequential Least Squares Quadratic Programming	based	
	GA	Genetic Algorithm	free	х
	NSGAII	Non-dominated Sorting GA II	free	X
	NSGAIII	Non-dominated Sorting GA III	free	X
	EpsMOEA	Steady-state Epsilon-MO EA	free	X
	MOEAD	MO EA based on Decomposition	free	X
EA	GDE3	Generalized Differential Evolution 3	free	X
	SPEA2	Strength Pareto EA 2	free	X
	IBEA	Indicator-Based EA	free	X
	PEAS	Parallel EAs	free	X
	PESA2	Pareto Envelope-based Selection Algorithm	free	X
	CMAES	Covariance Matrix Adaptation Evolution Strategy	free	
	ALPSO	Augmented Lagrangian PSO	free	
PSO	OMOPSO	Our multi-objective PSO	free	X
	SMPSO	Speed-constrained multi-objective PSO	free	X
	NOMAD	Non-linear Optimization by Mesh Adaptive Direct search	free	х
	SNOPT	Sparse Nonlinear OPTimizer	based	
041	CONMIN	CONstrained function Minimization	based	
Others	IPOPT	Interior Point OPTimizer	based	
	Nelder-Mead		free	
	COBYLA	Constrained Optimization BY Linear Approximation	free	

Other heuristic strategies have also been explored. A widely used one is Particle Swarm Optimization (PSO), which is inspired by the collective behaviour of swarms. Each candidate solution, called a particle, adjusts its position in the design space according to its own best experience and that of its neighbours, guided by a velocity update rule. In this way, the swarm progressively moves towards promising regions while still maintaining exploration capability. PSO has been applied to multi-objective formulations in floating offshore wind, showing good efficiency, although it can suffer from premature convergence when diversity within the swarm is lost.

While all these methods offer a wide range of capabilities, their suitability depends on the problem structure and the available computational resources. According to recent reviews, genetic algorithms remain by far the most widely adopted approach in floating offshore wind optimization, as shown in Figure 2.4 [28].

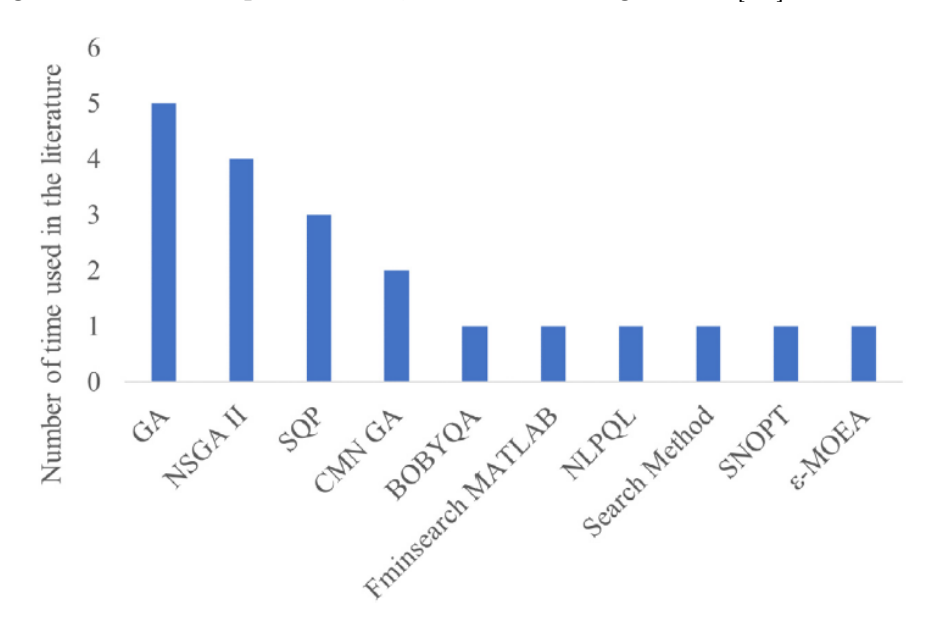


Figure 2.4: Optimisation algorithms used within the literature [28]

2.2.2 Genetic Algorithms (GA)

Genetic Algorithms (GAs) are among the most established heuristic optimisation methods and have been widely applied in the design and analysis of offshore wind systems. They operate on a population of candidate solutions (chromosomes), iteratively improved through evolutionary operators such as selection, crossover, and mutation. This balance of exploration and exploitation makes them particularly effective for complex, nonlinear, or multi-modal problems where deterministic methods often fail [7].

A standard GA can be described through the following cycle:

- 1. Initialization: generation of an initial population of candidate solutions, either randomly or with heuristics, ensuring sufficient diversity.
- 2. Fitness evaluation: assessment of each individual through the objective function, including constraint handling via penalties or repair mechanisms.
- 3. Selection: choice of parents according to performance, typically via roulette wheel (probability-based) or tournament (competition-based) schemes, with elitism preserving the best individuals.

- 4. Variation: creation of offspring through crossover (recombination of parent genes) and mutation (random perturbations), combining inheritance of good traits with exploration of new regions.
- 5. Replacement: formation of the new population (population update), after which the cycle is repeated until a stopping criterion is reached.

Over time, many multi-objective variants of GAs have been developed to approximate the Pareto front. As summarised in Table 2.1, these include a wide range of approaches. Early formulations such as MOGA, NPGA, and the original NSGA pioneered non-dominated sorting and niching strategies, but suffered from high computational cost and lack of elitism. Among later alternatives, the Strength Pareto Evolutionary Algorithm (SPEA) introduced elitism through an external archive of non-dominated solutions, while the Cumulative Multi-Niching GA (CMN-GA) combined clustering and elitism to improve convergence in multimodal landscapes. These examples illustrate the progressive refinement of GA-based methods, addressing limitations of the early algorithms and leading to more robust performance in multi-objective optimisation [9, 28].

A showed in Figure 2.4 the Non-dominated Sorting Genetic Algorithm II (NSGA-II) and in general GA remains the most widely adopted due to their robustness and computational efficiency [28].

NSGA-II [9] addressed the main drawbacks of earlier algorithms by introducing a fast non-dominated sorting procedure with reduced computational complexity, an explicit elitism mechanism through the combination of parent and offspring populations, and a diversity-preservation operator based on crowding distance, thus avoiding the need for arbitrary niching parameters. These features allow NSGA-II to converge efficiently while maintaining a well-distributed Pareto front, making it particularly suitable for large-scale, multi-objective engineering problems. For this reason, NSGA-II was selected in this thesis as the optimisation method and is further explained in the Methodology section.

3. Methodology

3.1 Workflow Overview

The optimization procedure developed in this work can be schematically represented as shown in Figure 3.1. Starting from the definition of the input parameters (geometry, environmental conditions, turbine characteristics and moorings) and the optimization setup, each candidate solution is evaluated through the objective functions. A constraint check is then performed, and only feasible designs contribute to the construction of the Pareto front. This workflow provides an overview of the internal logic of the optimization loop, which is further detailed in the following subsections.

In the present work, the evaluation of candidate designs is carried out in the static and frequency domain. The static analysis provides equilibrium checks under simplified load cases, ensuring that basic hydrostatic and stability conditions are satisfied. The frequency-domain analysis captures the linear response of the floating platform to harmonic wave excitation, allowing the estimation of key dynamic properties such as natural periods and response amplitude operators (RAOs). This approach offers a good compromise between accuracy and computational efficiency, making it possible to evaluate large populations of candidate solutions within reasonable time frames, which is essential for multi-objective genetic algorithm optimization.

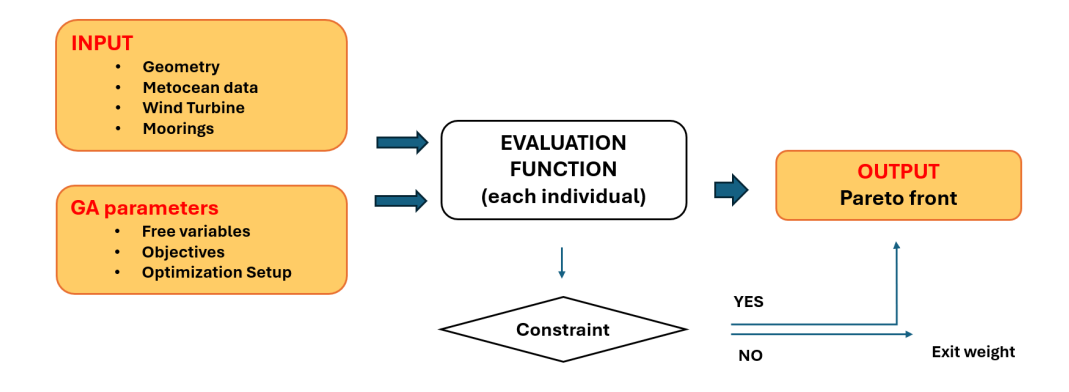


Figure 3.1: Workflow

3.2 Optimisation algorithm (NSGA-II)

The objective of this study is to identify the optimal combination of the main external geometric dimensions of the floating platform that best satisfies multiple technoeconomic and environmental performance objectives, while complying with predefined design and operational constraints. The optimization is carried out with the Non-dominated Sorting Genetic Algorithm II (NSGA-II), a widely adopted multi-objective evolutionary algorithm particularly suited to complex design spaces with conflicting objectives. Rather than searching for a single best design, NSGA-II approximates the trade-offs among objectives.

This work evaluates platform performance through two complementary assessments. The first is a techno-economic evaluation, based on the platform dynamic response (RAO indices), the capital expenditure (CAPEX), and the annual energy production (AEP). The second is a techno-economic–environmental evaluation, which integrates RAO indices with the Cost Over Productivity (COP) and the Equivalent CO₂ over Productivity (EOP), thus explicitly including environmental performance alongside technical and economic metrics.

As said, NSGA-II is selected for its ability to balance convergence and diversity through fast non-dominated sorting and a crowding distance operator, ensuring a well-distributed set of Pareto-optimal solutions [9].

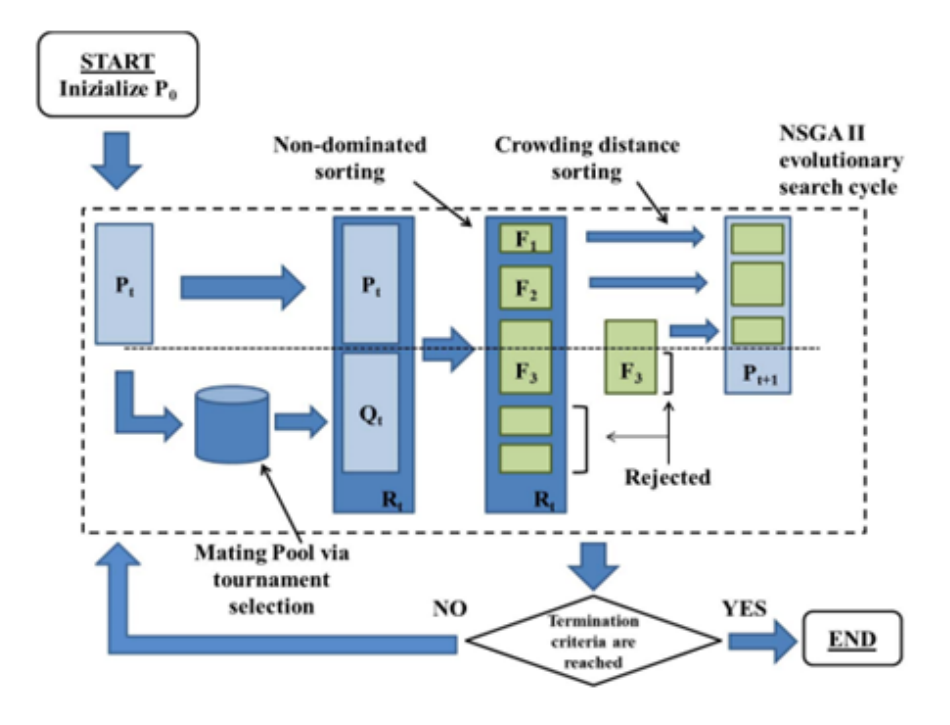


Figure 3.2: NSGA-II algorithm scheme

The main steps illustrated in Figure 3.2 of the NSGA-II algorithm, consistent with the general genetic algorithm framework, are carried out following the next steps.

Initialization

An initial population P_0 of N individuals is generated, with each individual representing a vector of decision variables \mathbf{x} within the problem's design space. Each individual is evaluated using the functions $f_{ev}(\mathbf{x})$, which compute the objective values and assess constraint violations.

The algorithm then applies Non-dominated Sorting to classify individuals into dominance based fronts (Figure 3.3). An individual S_1 dominates another S_2 if S_1 is at least as good as S_2 in all objectives and strictly better in at least one objective. In constrained optimization problems, feasible solutions always dominate infeasible ones. Among infeasible solutions, dominance is determined by comparing the total constraint violation, with smaller violations considered superior.

Solutions that are not dominated by any other individual constitute the first Pareto front. Those dominated only by individuals in the first front form the second front, and this procedure continues for subsequent fronts. Each solution is assigned a dominance rank Rank(i) corresponding to its front, where a lower rank indicates a better solution.

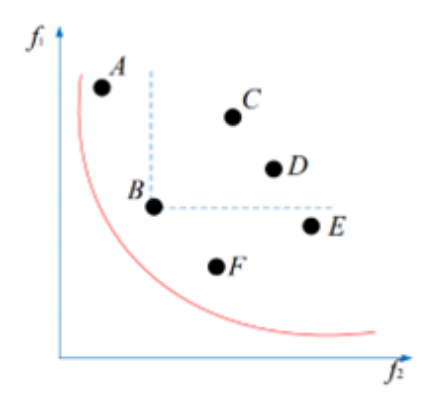


Figure 3.3: NSGA-II non dominated sorting

To promote diversity, individuals within each front are sorted based on their *crowding* distance, which estimates the density of solutions surrounding a given point in the objective space as shown in Figure 3.4. The crowding distance of an individual S_i within a front is calculated as:

Crowding Distance:
$$S_i = \sum_{k=1}^{M} \frac{\left| f_k^{(i-1)} - f_k^{(i+1)} \right|}{\text{Range}_k}$$
(3.1)

where $Range_k$ is the span of the objective k among all individuals in the front.

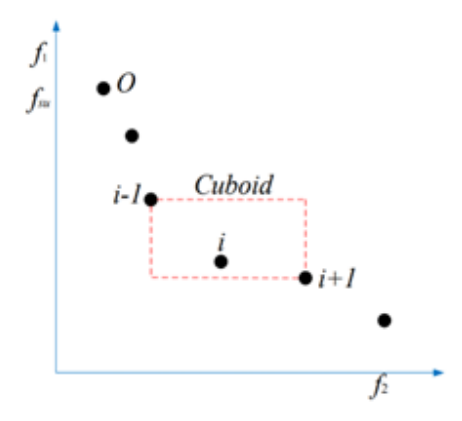


Figure 3.4: NSGA-II crowding distance

Parent Selection

Parents for the next generation are chosen through a process called binary tournament selection. This involves randomly grouping individuals into N sets (tournaments) of size M. Within each group, individuals are compared based on their dominance rank: the individual with the better (lower) rank wins. If there is a tie, the crowding distance is used as a tiebreaker, favoring individuals located in less crowded regions of the objective space to maintain diversity.

This selection method balances exploitation of the best solutions (those with low rank) and exploration of diverse solutions (those with higher crowding distance), thereby promoting a well-distributed and high-quality population for producing offspring.

Offspring Creation

New offspring (population Q) are created by applying Simulated Binary Crossover (SBX) to the selected parents. A fraction of individuals (defined by crossover probability p_C) are passed directly without modification, while the remaining are recombined using the following expressions.

Let x_{1i} and x_{2i} be the *i*-th decision variable of the two selected parents. The offspring

values Q_{1i} and Q_{2i} are computed as:

 $\beta = \text{random number from } [0, 1]$

$$\beta_{q} = \begin{cases} (2\beta)^{\frac{1}{\eta_{c}+1}} & \text{if } \beta \leq 0.5\\ (2(1-\beta))^{-\frac{1}{\eta_{c}+1}} & \text{if } \beta > 0.5 \end{cases}$$

$$Q_{1i} = 0.5 \left[(1+\beta_{q})x_{1i} + (1-\beta_{q})x_{2i} \right]$$

$$Q_{2i} = 0.5 \left[(1-\beta_{q})x_{1i} + (1+\beta_{q})x_{2i} \right]$$
(3.2)

Here, η_c is the distribution index, typically set between 5 and 20, which controls the spread of generated solutions.

Each decision variable x_i of the offspring is subjected to mutation with a probability p_m . If selected, a small perturbation δ is added, drawn from a Gaussian (or other) distribution:

$$x_i' = x_i + \delta \tag{3.3}$$

Here, x'_i is the mutated value. To ensure the new value remains valid, boundary handling methods may be applied if x'_i exceeds the allowed range.

The newly generated individuals are evaluated using the same functions $f_{ev}(\mathbf{x})$, in order to update objective values and constraint violations.

Environmental Selection

The current parent population P_t and the offspring population Q_t are merged into a combined population R_t of size 2N. A fast non-dominated sorting procedure is applied to assign a non-domination rank to each individual in R_t . Environmental selection then proceeds similarly to parent selection, by iteratively adding the best-ranked non-dominated fronts to the new population P_{t+1} until the total number of individuals reaches N.

If the last selected front exceeds the remaining slots, individuals within that front are sorted based on their crowding distance, and the top individuals are chosen to complete the new population. This mechanism ensures elitism by preserving the best solutions found so far, while also maintaining diversity across the objective space.

Termination Criteria

Repeat the steps of population creation and selection for a predefined number of generations G, or until a different termination condition is met. Possible termination conditions include:

- Convergence criteria met: The algorithm stops when the solutions found in successive generations do not significantly improve compared to those in previous generations. This indicates that the algorithm has reached stability, and further significant improvements are unlikely. Exit via this criterion is the most desirable, assuming the initial design domain is appropriately chosen.
- Maximum function evaluations reached: Termination occurs after computing
 the evaluation function a specified maximum number of times. This condition
 helps control computational resources, especially when function evaluations
 are computationally expensive.
- Diversity stagnation: The algorithm stops if the diversity of solutions remains constant or decreases significantly for a specified number of generations. Stagnation in diversity may indicate that the algorithm is trapped in a local minimum or is unable to effectively explore the solution space.
- Maximum elapsed time reached: The algorithm terminates after a predefined time period has elapsed. This condition helps control the total execution time of the algorithm and prevents prolonged execution in case of difficulties in finding better solutions.

These criteria ensure that the algorithm terminates within practical computational limits while providing a well-converged and diverse set of Pareto-optimal solutions.

3.3 Optimization objectives

The aim of this study is to explore how the design of a floating offshore wind platform can be optimised to achieve a balanced performance in terms of stability, cost efficiency, and environmental impact. These three aspects represent the main domains influencing the overall feasibility of floating wind technology: the technical domain reflects the hydrodynamic stability and motion behaviour of the system, the economic domain determines its affordability and competitiveness, and the environmental domain accounts for its contribution to decarbonisation targets through material and energy use.

To investigate the interplay among these domains, two separate optimisation studies are carried out:

- a techno-economic optimisation, focusing on the trade-off between platform stability and cost,
- a techno-environomic optimisation, extending the analysis to include environmental performance alongside stability.

This dual approach enables a comparative assessment of how design parameters influence not only the hydrodynamic behaviour of the platform but also its economic and environmental implications. The optimisation process seeks to explore how changes in geometry and material usage influence the different aspects simultaneously, providing a comprehensive picture of how engineering design choices affect both technical performance and long-term environmental and economic viability.

3.3.1 Technical objective

The technical objective focuses on assessing the dynamic stability of the floating platform, which is a fundamental requirement for its safe and reliable operation. The substructure must remain sufficiently stable to support the wind turbine tower, minimizing excessive motions that could compromise structural integrity, turbine performance, or control safety.

Under realistic operating conditions, the platform is subjected to periodic loads generated by wind and waves, which induce coupled motions in six degrees of freedom (6-DoF) shown in Figure 3.5: three translations (surge, sway, heave) and three rotations (roll, pitch, yaw).

In linear potential flow theory, the forces acting on the body are typically decomposed into excitation forces, arising from incident waves, and radiation forces, generated by the motion of the body itself. The *excitation forces* can be further separated into forces due to the undisturbed wave pressure on the body (Froude–Krylov), and the diffraction forces, which accounts for the modification of the wave field caused by the presence of the structure.

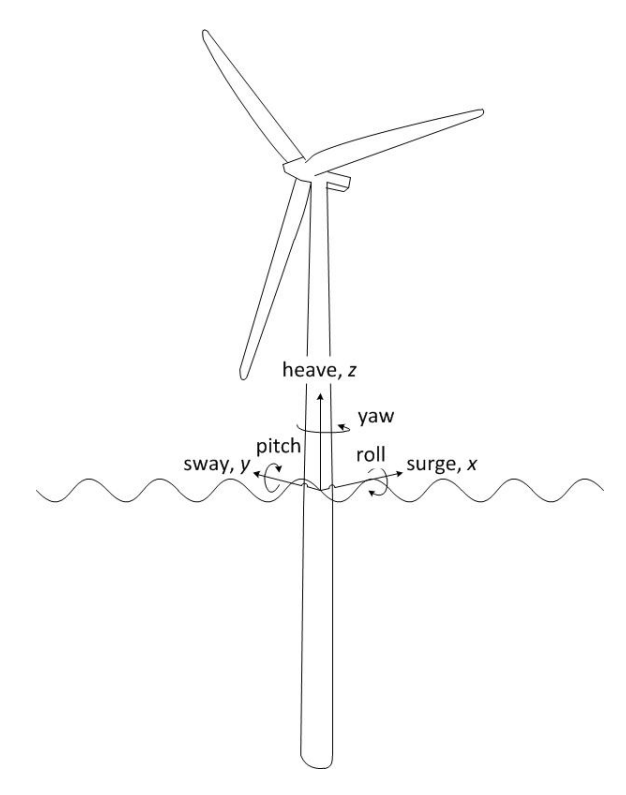


Figure 3.5: Offshore floating wind turbine platform degrees of freedom [10]

The radiation force, on the other hand, is associated with the waves radiated by the oscillating body. This reactive load can be expressed in terms of added mass, representing the inertia of the surrounding water moving with the body, and radiation damping, which accounts for the energy dissipated through the radiated waves.

In addition to these hydrodynamic contributions, the *hydrostatic restoring force* arises from Archimedes's principle. Acting proportionally to the displacement of the body, it can be expressed through the hydrostatic stiffness, acting as a linear spring that restores the system to its equilibrium position.

These contributions form the physical basis of the hydrodynamic problem. In the time domain, the general dynamics of a floating body are described by the Cummins equation [8], which in its simplified form can be written as

$$(m+A)\ddot{\xi}(t) + B\dot{\xi}(t) + K\xi(t) = \sum_{i=1}^{N} f_{\text{ext},i}(t)$$
 (3.4)

where m is the rigid-body mass, A the added mass, B the radiation damping, K the hydrostatic stiffness, and $f_{\text{ext},i}(t)$ the wave-excitation forces.

For multiple degrees of freedom these quantities are expressed as matrices. In the original formulation, radiation effects are represented through a convolution integral, which reduces to frequency-dependent added mass and damping terms under

harmonic oscillations.

In harmonic regime, the equation of motion for a single degree of freedom reduces to

$$\hat{\xi}(\omega) = \frac{\hat{F}_e(\omega)}{-\omega^2(m+a(\omega)) + i\omega b(\omega) + k}$$
(3.5)

where m is the rigid-body mass, $a(\omega)$ the added mass, $b(\omega)$ the radiation damping, k the hydrostatic stiffness, and $\hat{F}_e(\omega)$ the excitation force amplitude.

The Response Amplitude Operator (RAO) is then defined as the ratio between the response amplitude and the incident wave amplitude:

$$RAO(\omega) = \frac{\hat{\xi}(\omega)}{a_w} \tag{3.6}$$

with a_w the wave amplitude. The RAO therefore expresses the frequency-dependent sensitivity of the platform to incident waves.

From an optimisation perspective, the RAO is a particularly relevant parameter as it directly quantifies the dynamic amplification of surge, heave, and pitch, which are the most critical DoFs for floating wind applications. To ensure basic stability requirements, design constraints are imposed on peak RAO values so that individuals exhibiting excessive amplification are discarded during the optimisation process. Beyond its role as a constraint, the RAO is also employed as an objective function, guiding the optimisation towards more stable configurations and favouring the selection of designs with improved hydrodynamic performance in the final Pareto front.

Different RAO-based metrics can be found in the literature. Nacelle accelerations are often used as a proxy for turbine loads and drivetrain performance, while other studies employ the RAO of platform displacements (surge, heave, pitch) at natural frequencies as an indicator of global dynamic stability [22]. The two approaches are theoretically related in harmonic regime, since

$$RAO_{a,k}(\omega) = \omega^2 RAO_{p,k}(\omega)$$
 (3.7)

but they emphasise different frequency ranges and design aspects. In this work, the analysis is based on platform displacements, as they provide a direct measure of global stability and are more consistent with the adopted optimisation framework.

3.3.2 Economic objective

While ensuring dynamic stability is a key technical objective, economic feasibility is equally crucial for the competitiveness of floating offshore wind technology. As in most engineering applications, cost minimisation is the primary driver, making the identification of the cheapest feasible configuration essential to reduce costs while maintaining high energy yield.

The economic performance of a project is often assessed through the Levelised Cost of Energy (LCOE), defined as the ratio between the total discounted life cycle cost and the total discounted energy production:

$$LCOE = \frac{\sum_{t=1}^{N} \frac{CAPEX_{t} + OPEX_{t} + DECEX_{t}}{(1+r)^{t}}}{\sum_{t=1}^{N} \frac{AEP_{t}}{(1+r)^{t}}}$$
(3.8)

where $CAPEX_t$, $OPEX_t$, and $DECEX_t$ are respectively the capital, operational, and decommissioning expenditures at year t, AEP_t is the annual energy production, r is the discount rate, and N is the project lifetime in years.

Since LCOE reflects the cost of a unit of energy produced, lowering its value is beneficial for electricity consumers and improves the competitiveness of wind energy in the market. A lower LCOE can be achieved by either increasing energy production or reducing the costs.

The productivity of the turbine is quantified through the Annual Energy Production (AEP), which represents the net amount of electricity generated in one year under site-specific wind conditions, accounting for wake losses, availability, and other operational factors. In general, AEP can be expressed as:

$$AEP = \int_0^\infty P(v) f(v) dv$$
 (3.9)

where:

- P(v) is the power output of the turbine at wind speed v (power curve),
- f(v) is the probability density function of the wind speed distribution at the site.

In discrete form, this becomes:

$$AEP = 8760 \sum_{i=1}^{N} P(v_i) \ p(v_i)$$
 (3.10)

where $p(v_i)$ is the probability of occurrence of wind speed v_i , and 8760 is the number of hours in a year.

In the literature, the LCOE of offshore floating wind projects is shown to depend on a broad set of cost drivers. The most significant factors include:

- Manufacturing costs: typically divided into wind turbines, platforms, transmission systems, and mooring/anchoring. Among these, the mass of steel and fabrication complexity are usually the dominant CAPEX drivers, being directly linked to platform geometry. Mooring and anchoring systems are especially relevant for TLPs and similar concepts, as their design strongly influences both cost and installation effort. Export cables and substations can also represent a substantial cost share, highly dependent on the distance to shore.
- Installation strategies and farm size: large projects and efficient assembly methods enable economies of scale, whereas suboptimal logistics or vessel use can significantly increase total costs.
- Operation and maintenance (O&M): costs are sensitive to offshore distance, site accessibility, and maintenance strategy (preventive, corrective, or condition-based), and thus play a crucial role in the lifetime economics of the project.
- Decommissioning: although usually a smaller component, decommissioning costs can still be relevant depending on material recovery, recycling, and disposal strategies.

Several techno-economic assessments confirm that CAPEX remains the dominant component of the LCOE for floating offshore wind turbines, with the substructure cost representing the largest share of investment [29]. Myhr et al. [20] showed that even when considering different floating concepts (spar, semisub, TLP), the relative weight of OPEX and DECEX is modest compared to the initial capital investment. This further supports the focus on platform-related CAPEX as the primary economic driver in optimisation studies. In this thesis, only the capital cost associated with the floating platform design is allowed to vary, whereas other cost

components are assumed fixed. A simplified measure of LCOE is therefore adopted within the optimisation loop, as described later in the chapter.

3.3.3 Environmental objective

While techno-economic assessments are the standard reference for evaluating floating offshore wind projects, only a limited number of studies have extended the analysis to include environmental indicators such as life-cycle greenhouse gas emissions or energy payback metrics [24, 11]. Incorporating these aspects provides valuable complementary information, especially considering that material requirements for the substructure and mooring systems strongly influence the overall environmental footprint.

In Life Cycle Assessment (LCA), the environmental impact is typically quantified in terms of greenhouse gas (GHG) emissions expressed as CO₂-equivalent, normalized either per unit of installed capacity [tCO₂/MW] or per unit of energy generated [gCO₂/kWh]. This allows the comparison of different technological configurations and their alignment with decarbonisation pathways.

Previous LCA studies on offshore wind concepts have shown that the environmental and economic performances share common drivers. The structural steel mass of the substructure represents the dominant contribution to both CAPEX and embodied GHG emissions. For instance, Raadal et al. [24] quantified that a 1% increase in platform steel mass results in an increase in total life-cycle GHG emissions between 0.12% and 0.5%, depending on the concept. Mooring lines and anchors add a smaller but non-negligible contribution that depends on concept and materials. In addition, installation and decommissioning activities can account for 18–33% of total GHG emissions, reflecting the energy use of marine operations.

While the structural mass of the platform establishes a strong proportionality between cost and emissions, additional components such as mooring and anchors introduce a more complex relationship. Installation and decommissioning processes further amplify this effect, as they can significantly increase both CAPEX and emissions depending on logistics and fuel consumption. Also As a result, a degree of decoupling between economic and environmental objectives can already emerge when these factors are considered. In this context, the addition of an environmental objective to the economic one is useful to highlight trade-offs between cost and carbon intensity, allowing design solutions to be assessed not only in terms of financial viability but also with respect to their contribution to decarbonisation targets.

3.4 Metocean conditions

Wave conditions

Common types of wave spectra are Pierson–Moskowitz (PM) and JONSWAP. In this context, the JONSWAP spectrum is employed to determine the unidirectional irregular sea state condition. The general form of a wave spectrum is:

$$S_w(\omega) = A_{ws} \,\omega^{-5} \,\exp\left(-B_{ws} \,\omega^{-4}\right) \tag{3.11}$$

where A_{ws} and B_{ws} are coefficients that vary depending on the spectrum.

The PM spectrum is applicable to a fully developed sea when the growth of the waves is not limited by the fetch [23]. It is defined as:

$$S_{PM}(\omega) = \frac{H_s^2}{4} \left(1.057 \,\omega_p \right)^4 \omega^{-5} \,\exp \left[-\frac{5}{4} \left(\frac{\omega_p}{\omega} \right)^4 \right] \tag{3.12}$$

where H_s is the significant wave height and $\omega_p = 1/T_p$ is the inverse of the peak period.

The JONSWAP spectrum is formulated as a modification of the PM spectrum for a developing sea state in a fetch-limited situation. The spectrum accounts for a higher peak and a narrower bandwidth in a storm situation for the same total energy as compared to the PM spectrum. The spectral density of the surface elevation defined by the JONSWAP spectrum [15] is:

$$S(\omega) = C_{ws} S_{PM}(\omega) \gamma^{\alpha}$$
(3.13)

with

$$C_{ws} = \frac{\int_0^\infty S_{PM}(\omega) d\omega}{\int_0^\infty S_{PM}(\omega) \gamma^\alpha d\omega} = 1 - 0.287 \ln(\gamma), \tag{3.14}$$

$$\alpha = \exp\left[-\frac{\left(\frac{\omega}{\omega_p} - 1\right)^2}{2\sigma^2}\right], \quad \sigma = \begin{cases} 0.07 & \text{if } \omega < \omega_p \\ 0.09 & \text{if } \omega > \omega_p \end{cases}$$
(3.15)

$$\gamma = \begin{cases}
5 & \text{if } \frac{T_p}{\sqrt{H_{m0}}} \le 3.6 \\
\exp(5.75 - 1.15 \, T_p / \sqrt{H_{m0}}) & \text{if } 3.6 < \frac{T_p}{\sqrt{H_{m0}}} < 5 \\
1 & \text{if } \frac{T_p}{\sqrt{H_{m0}}} \ge 5
\end{cases} \tag{3.16}$$

The spectral density $S(\omega)$ refers to a specific sea state. However, since the optimisation aims to account for the metocean conditions of the target site, the objective is evaluated over the entire scatter diagram of sea states observed during the last N years. This diagram expresses the occurrence probabilities of the various sea states, each characterised by a peak period T_p and a significant wave height H_s .

For each sea state, the spectral density $S(\omega)$ is described by the JONSWAP formulation. This spectral model is consistently used for the evaluation of both constraints and objectives in the optimisation framework.

Wind conditions

Wind regime represents a fundamental input for the optimisation process, since it directly influences the Annual Energy Production (AEP). Wind speed measurements are typically available at a reference height z_{ref} (e.g., 100 m above sea level) and must be extrapolated to the hub height z_{hub} of the turbine. This extrapolation can be performed either using the logarithmic law, which accounts for atmospheric stability and surface roughness, or the simpler power law, expressed as:

$$U(z) = U(z_{ref}) \left(\frac{z}{z_{ref}}\right)^{\alpha} \tag{3.17}$$

where U(z) is the wind speed at height z, and α is the wind shear exponent, typically ranging between 0.1 and 0.2 in offshore environments [6].

To represent the long-term variability of the wind, the statistical distribution of wind speeds is generally described by a Weibull probability density function:

$$f(U) = \frac{k}{c} \left(\frac{U}{c}\right)^{k-1} \exp\left[-\left(\frac{U}{c}\right)^{k}\right],\tag{3.18}$$

where k is the shape parameter and c is the scale parameter. This distribution is commonly used to estimate the wind occurrence and, combined with the turbine power curve, allows for the evaluation of the expected energy yield.

3.5 Evaluation function

In this section, the evaluation function is described. It takes as input the characteristics of the individuals to be assessed at each iteration and performs a sequence of operations to compute the corresponding objective values and constraint violations. These results are then used to carry out the environmental selection phase.

The function first adjusts the design variables, if necessary, to ensure compliance with the imposed bounds. It then calls the CAD software SALOME to generate the geometry and compute the corresponding inertial and hydrostatic properties. Subsequently, the hydrodynamic solver Nemoh is executed to obtain the relevant hydrodynamic coefficients. Its outputs, together with those from an external technoenvironmental performance model (FLOWTEM), which is used to estimate farmlevel metrics such as cost and carbon emissions, are combined to calculate the final objective values and constraint violations.

The following figure illustrates the overall workflow of the evaluation process, while the subsequent subsections detail each of the steps involved.

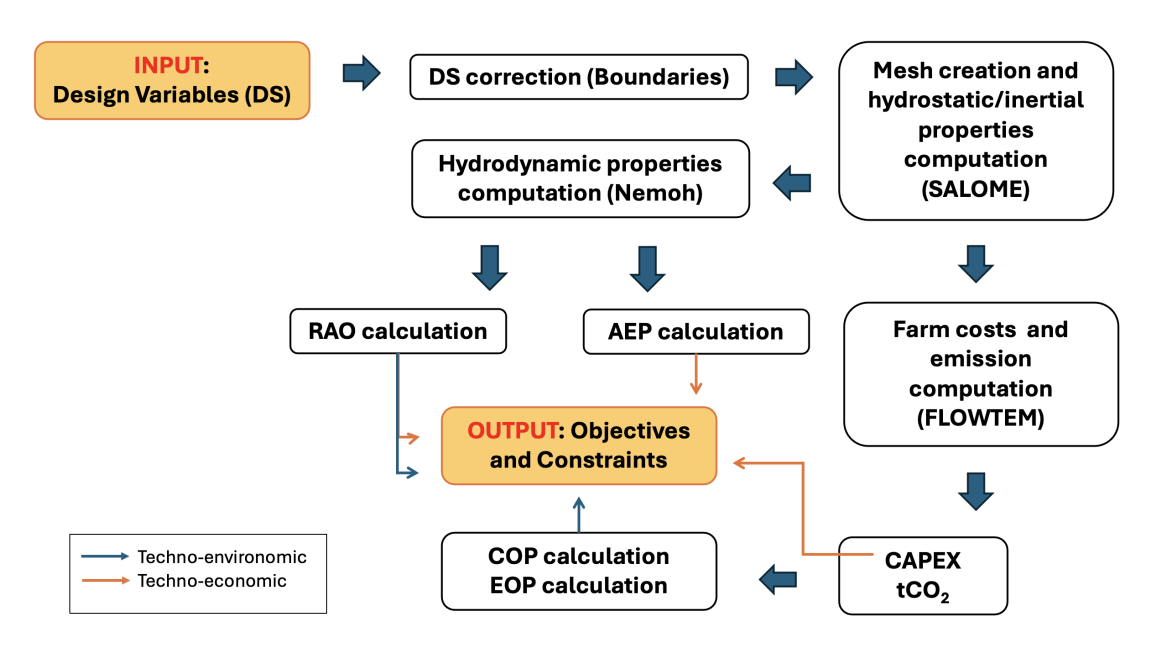


Figure 3.6: Evaluation function workflow

3.5.1 Geometry generation and hydrostatics (SALOME)

For the evaluation of each individual, it is necessary to generate a consistent CAD model of the floating platform and to compute its associated hydrostatic and inertial properties. To this end, the CAD software SALOME is employed within the optimization loop, enabling parametric geometry creation and the automated calculation of key physical quantities such as mass distribution and restoring stiffness. Its integration ensures that the design variables provided by the genetic algorithm are translated into physically consistent data for subsequent hydrodynamic analyses.

SALOME is an open-source platform for CAD modeling and preprocessing, developed by the collaboration between Électricité de France (EDF) and the Commissariat à l'énergie atomique et aux énergies alternatives (CEA). The software provides advanced solid and surface modeling tools, but its main strength lies in its full Python integration, which allows operations to be reproduced through automatically generated scripts. This capability makes it particularly suited for optimization frameworks, as it enables parametric geometry definition, custom equations (e.g., hydrostatic equilibrium, ballast mass computation), and fully automated workflows.

In this project, SALOME (v9.13.0) supports the evaluation process in three main aspects:

- Parametric geometry generation directly linked to the design variables, including the external solid body for hydrostatics, the submerged volume for buoyancy, the waterplane area for inertia, and the hydrodynamic shell for meshing;
- 2. Computation of mass and inertia properties, including the ballast required to satisfy draft and freeboard constraints, as well as the center of gravity (COG) and inertia tensor;
- 3. Export of matrices and mesh, specifically the mass matrix M, the hydrostatic stiffness matrix K_{hydro} , and the hydrodynamic panel mesh required for subsequent NEMOH analyses.

The hydrostatic stiffness accounts for restoring forces and moments due to buoyancy, including additional restoring contributions when $COG \neq COB$. These outputs $(M, K_{hydro}, \text{ mesh})$ are fundamental inputs for the following hydrodynamic analysis and directly influence stability, natural periods, RAOs, and ultimately the techno-economic and environmental performance indicators.

3.5.2 Hydrodynamic analysis (NEMOH)

Once the geometry and hydrostatic properties are defined in SALOME, the evaluation loop proceeds with the computation of hydrodynamic coefficients through NEMOH. This step provides the dynamic response of the platform under wave excitation, which is essential for assessing motion constraints and performance objectives in the optimization.

NEMOH (v3.0) is a numerical solver for wave—structure interaction problems based on the Boundary Element Method (BEM) in the frequency domain. In BEM, only the boundaries of the body and free surface are discretized, reducing computational cost compared to volume-based approaches. NEMOH contains two main modules: the first, Nemoh1, solves linear diffraction and radiation problems of wave—structure interaction using BEM in the frequency domain; the second, Nemoh2, extends the analysis to second-order effects by computing difference- and sum-frequency Quadratic Transfer Functions (QTFs) for fixed or floating structures. Within this project, only first-order analyses (Nemoh1) are considered, as they are sufficient to evaluate platform motions and related constraints during optimization.

The solver is fully integrated into the MATLAB workflow through automated scripts that handle the following tasks:

- Conversion of the hydrodynamic mesh generated in SALOME into NEMOH format;
- 2. Automatic generation of input files (Nemoh.cal, Mesh.cal);
- 3. Execution of the NEMOH solvers (preProc.exe, solver.exe, postProc.exe);
- 4. Import of hydrodynamic coefficients, including added mass (A), radiation damping (B), and wave-excitation forces (f_{ext}) .

These coefficients are combined with the mass and stiffness matrices from SALOME to calculate natural frequencies and RAOs. By coupling SALOME for hydrostatics and NEMOH for hydrodynamics, the evaluation function ensures a balance between physical accuracy and computational efficiency, allowing the genetic algorithm to explore the design space effectively.

3.5.3 Constraints

When designing motion constraints for floating platforms, the primary goal is to maintain stability, structural integrity and avoid impacts on power production. Constraints can be imposed on the various degrees of freedom (DoF), with the static pitch angle typically being the most significant, since excessive pitch may reduce the turbine's aerodynamic efficiency and, in extreme cases, threaten platform stability. Limits on other motions are also imposed to prevent excessive displacements that could overload mooring lines or export cables. Additionally, platform motions are evaluated with respect to their natural periods and frequencies to ensure that they remain sufficiently separated from the energetic wave spectrum, avoiding resonance phenomena under the specific environmental conditions.

For Tension-Leg Platforms (TLPs), the static pitch angle is generally less critical than for other floating concepts, as pitch motions are inherently small due to the vertical mooring system. In standard practice, the static pitch constraint is evaluated by considering the maximum thrust force acting on the wind turbine and checking the resulting pitch angle for several yaw positions of the Rotor Nacelle Assembly. In this study, a simplified approach is adopted: the static pitch is assessed by computing the platform's equilibrium pitch under the given loads and comparing it to a predefined allowable limit. This simplification is justified by the limited pitch motions of TLPs and provides a conservative safeguard without the need for a full yaw-dependent analysis and so saving computational time.

The main motion constraints considered in this study are therefore related to the natural frequencies and the mooring system, ensuring that platform motions remain within acceptable bounds. This prevents resonance with incoming waves, excessive line loading, or slack in the mooring system, which could compromise both stability and structural integrity. If the constraints are violated, a corresponding penalty value is assigned to the individual and combined according to predefined weights to form an overall exit score, which lead the individual to be discarded from the optimization process. This approach ensures that only individuals satisfying all motion constraints are propagated in the selection. The method is applied consistently across all constraints, including static pitch, natural periods and frequencies, and mooring line tensions.

Resonance constraint

The resonance constraint ensures that the natural frequencies of the floating platform are sufficiently far from the dominant wave frequencies at the deployment site to avoid resonance conditions that could amplify the motions of the platform.

From a preliminary JONSWAP analysis at the site, the most energetic wave periods are identified and converted into forbidden ranges for platform natural periods. These are expressed as bounds $T_{\lim,j}$ with an associated sign vector $s_j \in \{-1, +1\}$ that encodes the inequality direction $(s_j = +1 \text{ for lower bounds } T_{n,j} \geq T_{\lim,j}; s_j = -1 \text{ for upper bounds } T_{n,j} \leq T_{\lim,j})$. The constraint metric used in the optimization is:

$$Cons_{res} = \max_{j} s_j (T_{n,j} - T_{\lim,j}), \qquad (3.19)$$

and feasibility requires $Cons_{res} \leq 0$. In practice, this enforces heave and pitch to remain below prescribed thresholds and surge/sway above minimum values, ensuring sufficient separation from the energetic wave bands without explicitly integrating the spectrum around ω_n .

For each individual, the natural frequencies are obtained by solving the following eigenvalue problem:

$$\left(K - \omega_n^2 \left(M + A_\infty\right)\right) \phi = 0 \tag{3.20}$$

where ω_n is the vector of natural frequencies, ϕ contains the eigenvectors, M is the mass matrix of the system (turbine + platform), K is the stiffness matrix ($K = K_{\text{hydro}} + K_{\text{mooring}}$), and A_{∞} is the infinite-frequency added mass matrix.

In the script, the natural frequencies of the platform in the heave and pitch DoF are calculated as:

$$\omega_n = \sqrt{\frac{\operatorname{diag}(K)}{\operatorname{diag}(M + A_\infty)}}, \qquad T_n = \frac{2\pi}{\omega_n}$$
(3.21)

If $Cons_{res} > 0$, the constraint is violated and the design is considered infeasible. This methodology prevents platform resonance without explicitly integrating the spectrum around the natural frequency, providing a computationally efficient and robust evaluation.

Overall, this approach guarantees that the natural periods in heave and pitch are kept outside the most energetic sea states, reducing the risk of resonance and providing a safe starting point for further hydrodynamic optimization.

Moorings constraint

The design of a Tension Leg Platform (TLP) is not self-stable without a mooring system. Therefore, a preliminary mooring system is implemented to evaluate the static pitch and the frequency-domain response of the platform. This initial mooring model allows the enforcement of key design constraints without to enforce design constraints without resorting to full nonlinear dynamic simulations.

A simplified mooring stiffness matrix K_{moor} is constructed from the platform geometry and the axial stiffness of the mooring lines, following the formulation proposed by Al-Solihat and Nahon [3], where the linearized restoring coefficients are derived from the catenary equilibrium configuration and assembled into a global stiffness representation suitable for frequency-domain analysis. The matrix provides an estimate of the restoring forces and moments contributed by the mooring system in each degree of freedom.

The net vertical force acting in the equilibrium configuration, defined as:

$$F_{\text{Net}} = F_b - F_q + F_{\text{net},b}^{\text{moor}} \tag{3.22}$$

where F_b is the downward ballast force, F_g is the structural weight of the platform, and $F_{\text{net},b}^{\text{moor}}$ is the vertical restoring component from the mooring lines.

The stiffness matrix is then expressed as:

$$K_{11}^{\text{moor}} = \frac{F_{\text{Net}}}{FL_D} \tag{3.23}$$

$$K_{15}^{\text{moor}} = \frac{F_{\text{Net}} F L_Z}{F L_D} \tag{3.24}$$

$$K_{22}^{\text{moor}} = \frac{F_{\text{Net}}}{FL_D} \tag{3.25}$$

$$K_{24}^{\text{moor}} = \frac{F_{\text{Net}} F L_Z}{F L_D} \tag{3.26}$$

$$K_{33}^{\text{moor}} = \frac{4EA}{L} \tag{3.27}$$

$$K_{44}^{\text{moor}} = \frac{F_{\text{Net}} F L_Z^2}{F L_D} + \frac{4 E A}{L} F L_Y^2$$
 (3.28)

$$K_{42}^{\text{moor}} = K_{24}^{\text{moor}}$$
 (3.29)

$$K_{55}^{\text{moor}} = \frac{F_{\text{Net}} F L_Z^2}{F L_D} + \frac{4 E A}{L} F L_X^2$$
 (3.30)

$$K_{51}^{\text{moor}} = K_{15}^{\text{moor}}$$
 (3.31)

$$K_{66}^{\text{moor}} = \frac{F_{\text{Net}} \left(F L_X^2 + F L_Y^2 \right)}{2 F L_D} \tag{3.32}$$

Here, FL_D is the distance from the fairlead to the seabed, FL_Z the distance from still water level to the fairlead, FL_X and FL_Y are the arm dimensions, n is the number of mooring lines, and EA is the line axial stiffness.

The consistency of this simplified stiffness formulation was verified by comparing its predictions with the results obtained from the numerical tool MOST. The comparison confirmed that the stiffness characteristics derived from the analytical approach provide a reliable representation of the mooring restoring behavior, thereby supporting its use in the present frequency-domain analysis.

To ensure platform stability and mooring functionality, the mooring system must satisfy simultaneously the following constraints:

- 1. Resonance constraints: the natural periods of the platform must remain outside the energetic wave bands as explained in the previous section.
- 2. Strength constraint: the maximum line tension must remain below the Mini-

mum Breaking Load (MBL). A worst-case tension is estimated as

$$T_{\text{max}} = \frac{F_T \cdot S_f \cdot (h_{hub} + FL_Z) - F_g(FL_X - x_{COG}) + F_b(FL_X + x_{COB}) + F_{b,\text{net}}FL_X}{2FL_X}$$

with a safety factor $S_f = 1.25$ to account for dynamic amplification. The design condition is

$$T_{\max} S_f^{MBL} \le \text{MBL}.$$

A preliminary elasticity EA is then estimated from the resonance constraints. For heave, the required mooring stiffness is obtained from the target natural period:

$$T_3^{\text{max}} = 2\pi \sqrt{\frac{M_{33} + A_{33}}{K_{33}^{\text{hydro}} + K_{33}^{\text{moor}}}} \le T_{3,\text{lim}}$$
 (3.33)

$$K_{33}^{\text{moor}} = \frac{M_{33} + A_{33}}{\left(\frac{T_3^{\text{max}}}{2\pi}\right)^2} - K_{33}^{\text{hydro}}$$
(3.34)

$$EA_3 = \frac{L}{n} K_{33}^{\text{moor}} \tag{3.35}$$

For the pitch, the restoring moment includes both the mooring contribution and a hydrostatic correction term due to the net buoyancy—weight couple:

$$T_5^{\text{max}} = 2\pi \sqrt{\frac{I_{55} + A_{55}}{K_{55}^{\text{hydro}} + K_{55}^{\text{moor}}}} \le T_{5,\text{lim}}$$
 (3.36)

$$K_{55}^{\text{moor}} = \frac{I_{55} + A_{55}}{\left(\frac{T_5^{\text{max}}}{2\pi}\right)^2} - K_{55}^{\text{hydro}}$$
(3.37)

$$EA_5 = \left(K_{55}^{\text{moor}} - \frac{F_b^{net} F L_Z^2}{F L_D}\right) \frac{L}{n F L_X^2}$$
 (3.38)

where M_{33} is the rigid-body mass term, A_{33} the added mass, K_{33}^{hydro} and K_{55}^{hydro} the hydrostatic stiffness terms, I_{55} the pitch inertia, A_{55} the added inertia, F_b^{net} the net buoyancy force, and FL_Z , FL_D , FL_X the relevant geometric dimensions.

In addition, a minimum stiffness EA_{MBL} is defined from the strength requirement through the manufacturer's MBL(EA) curve. The selected elasticity is therefore

$$EA = \max\left(EA_3, EA_5, EA_{\text{MBL}}\right) \tag{3.39}$$

From the chosen elasticity, the corresponding mooring line diameter is obtained by interpolation of manufacturer data. If the required cross-sectional area exceeds the maximum allowable diameter for a single line, the area is redistributed into multiple parallel strands of reduced diameter, preserving the same axial stiffness while ensuring geometric feasibility.

Because the draft is a design variable, the mooring length L must be iteratively adjusted to close the vertical equilibrium of each individual. An outer loop updates L and recomputes both EA and the corresponding line diameter until the mismatch on the net vertical force falls below a tolerance. In this way, both stiffness, length and diameter are consistently determined with the platform draft, while ensuring compliance with resonance, strength, and no-slack constraints. The resulting properties are finally used to assemble $K_{\rm moor}$ and to evaluate static pitch and RAOs in the subsequent frequency-domain analysis.

3.5.4 Objective evaluation

RAO-based Motion Metric

This objective is related to the performance of the platform; specifically, it expresses the magnitude of the platform's motion in the presence of waves and penalises those individuals that exhibit larger displacements under the same inputs. As specified before, the only degrees of freedom of interest for this study are surge, heave and pitch, as they are the most relevant to quantify the stability of a floating wind platform.

The objective function chosen is based on a combination of the Response Amplitude Operator (RAO), the spectral representation of irregular waves for given sea states, and the statistical occurrence of these sea states at the selected site. To this end, the RMS (Root Mean Square) value of the amplitude of the j-th degree of freedom of motion caused by an irregular sea condition is:

Amplitude_{RMS} =
$$\sqrt{\int_0^\infty |\xi_j(\omega)|^2 S(\omega) d\omega}$$
 (3.40)

where ξ_j is the RAO of the j-th degree of freedom and $S(\omega)$ is the wave spectrum.

The JONSWAP spectrum, previously introduced, is employed here to describe the energy distribution of irregular waves for each sea state. To account for realistic site-specific conditions, the optimisation is based on a weighted average over the full scatter diagram of sea states (see Figure 4.7).

The final objective value is then a weighted average according to both the probability

of occurrence of each sea state and the relative importance assigned to the considered degrees of freedom. To combine contributions expressed in different units, the RAOs are normalised with respect to the values obtained for the reference platform in each degree of freedom. In line with the chosen approach, the RAO of platform displacements (position) is employed in this study, consistently with a strand of literature focusing on global stability indicators.

The resulting objective function can be expressed as:

$$Obj_{RAO} = \sum_{k} W_k \cdot \left(\sum_{i} p_i \cdot \sqrt{\int_0^\infty \frac{|\xi_k(\omega)|^2}{|\xi_{ref,k}|^2} S_i(\omega) d\omega} \right)$$
(3.41)

where W_k is the weight for the k-th degree of freedom, ξ_k is the RAO of the k-th d.o.f., while S_i and p_i are respectively the wave spectrum and the probability of the i-th sea state.

COP-based Cost Metric

As already discussed, capital expenditure is the dominant component of floating wind costs. In the techno-economic optimisation, the economic objective is therefore represented explicitly by the CAPEX together with AEP. In the techno-economic–environmental optimisation, instead, these two quantities are aggregated into the *Cost Over Productivity index (COP)*, defined as:

$$COP = \frac{CAPEX}{AEP} \tag{3.42}$$

As described in the previous subsections, the AEP is obtained from wind resource data and pre-computed power curves as a function of the platform pitch stiffness. In practice, the relationship is approximated by a polynomial fit:

$$AEP(\theta) = \sum_{j=0}^{N} c_j \, \theta^j \tag{3.43}$$

where for each static pitch angle θ_j the c_j are the polynomial coefficients obtained from regression and N is the order of the polynomial.

The CAPEX is estimated through the farm-based scaling of the CAPEX calculated by the external techno-economic model FLOWTEM.

The CAPEX extracted is:

$$C_{farm} = C_{const} + N\left(1 + MCF\right) M_p \left(\sum_i f_i p_i\right)$$
(3.44)

where:

- C_{const} is the fixed contribution accounting for non-platform items (turbine, installation, transmission, and auxiliary systems),
- N is the number of turbines,
- *MCF* is a manufacturing complexity factor,
- M_p is the mass of the platform per turbine,
- f_i are the mass fractions of the different materials,
- p_i are the corresponding unit costs [\mathfrak{C}/t].

Then the results are scaled to the single-platform level and the contribution of the moorings is added:

$$C_{\text{plat}} = C_{\text{farm}} P_r \frac{M_{\text{plat}}}{\bar{M}_{\text{plat}}} + C_{\text{moor}}$$
(3.45)

where:

- P_r is the turbine rated power,
- $M_{\rm plat}$ is the mass of the candidate platform,
- $\bar{M}_{\rm plat} = M_{\rm farm}/N$ is the average platform mass in the farm,
- $C_{\text{moor}} = M_{moor} c_{moor}$ is the mooring cost of the candidate platform, with c_{moor} the unit costs of the moorings.

Emissions Metric

In the techno-economic—environmental optimisation, a third objective is introduced to account for the environmental impact of the floating platform, expressed in terms of greenhouse gas (GHG) equivalent emissions. Accordingly, the environmental objective is represented by the *Emissions Over Productivity index (EOP)*, defined as

$$EOP = \frac{Emissions}{AEP} \tag{3.46}$$

Here, Emissions represent the life-cycle equivalent carbon dioxide associated with the platform, approximated through a mass-based proxy of its main components, while the AEP is computed as in Equation 3.43 Analogously to COP, this formulation allows a direct comparison between different designs in terms of their carbon intensity per unit of electricity produced.

As for CAPEX, carbon emissions are evaluated in the techno-economic model using scaling relations derived from reference studies and assumptions. In particular, the mass of steel used in pontoons, columns, and braces is converted into tCO_{2eq} using emission factors from the literature. These values are then normalized by the expected energy production to obtain the objective indicator. Within the present optimisation framework, the environmental objective is formulated as the minimisation of the embodied CO_2 emissions of the platform. A simplified proxy is adopted, assuming emissions proportional to the total platform mass M_p , with an additional constant contribution accounting for the turbine, transport, and auxiliary systems:

$$CO_{2, tot} = CO_{2, const} + N M_p \left(\sum_i f_i e_i\right)$$
 (3.47)

where N is the number of units in the farm, f_i are the material mass fractions, and e_i their emission factors [kgCO₂/t].

To ensure consistency with the economic formulation, emissions are scaled from the farm-level reference values provided by FLOWTEM, proportionally to the platform mass. Unlike the CAPEX calculation, mooring-related contributions are not explicitly included here.

This provides a first-order estimate of environmental impact that primarily reflects the role of platform mass, while remaining computationally efficient. The formulation can be readily extended in future work to include further life-cycle contributions for more detailed optimisation.

4. Input Data & Case Study

4.1 Geometry

The floating support structure considered in this work is the GICON-SOF TLP, a tension-leg platform concept developed by GICON. The SOF combines features of semi-submersible and TLP systems, consisting of a buoyant substructure anchored to the seabed through pre-tensioned tendons. This hybrid design leverages the high stability typical of TLPs while maintaining construction and installation flexibility. The reference configuration analyzed in this thesis is designed to host a 15 MW wind turbine. The platform has a square-shaped base formed by four cylindrical pontoons, each with a diameter of $D_P = 10$ m, connected at the corners with rounded joints. The base measures are $L_x = 70$ m in the longitudinal direction and $L_y = 60$ m in the transversal direction.

A large vertical cylindrical column of $D_{WT}=9$ m diameter is attached to the midpoint of one side pontoon, serving as the main support for the wind turbine tower. From the upper part of this column, two inclined tubular braces extend diagonally towards the base pontoons. These elements enhance global stiffness and efficiently distribute turbine loads to the floating foundation. The joints between pontoons, braces, and the central column are smoothly connected to improve structural integrity and hydrodynamic behavior. On the side of the base opposite to the turbine, a ballast section of length $L_{Ballast}=5.2$ m is integrated. This component is essential for adjusting the center of gravity and enhancing the hydrostatic restoring moment. Figure 4.1 illustrates the reference geometry as implemented in the CAD model.

The reference draft is Draft = 38 m. Eight pre-tensioned tendons, each with a pretension force of about 102 MN, are anchored to the seabed at depths ranging from 60 to 150 m to ensure station-keeping and limit pitch, roll, and heave motions under operational and extreme environmental conditions.

Structural thicknesses of the different components, including columns, pontoons, braces, and end prisms, have been set according to reference values to preserve structural feasibility. This base configuration has been verified with external software and tools and is used in the initial population to guide the generation of individuals that

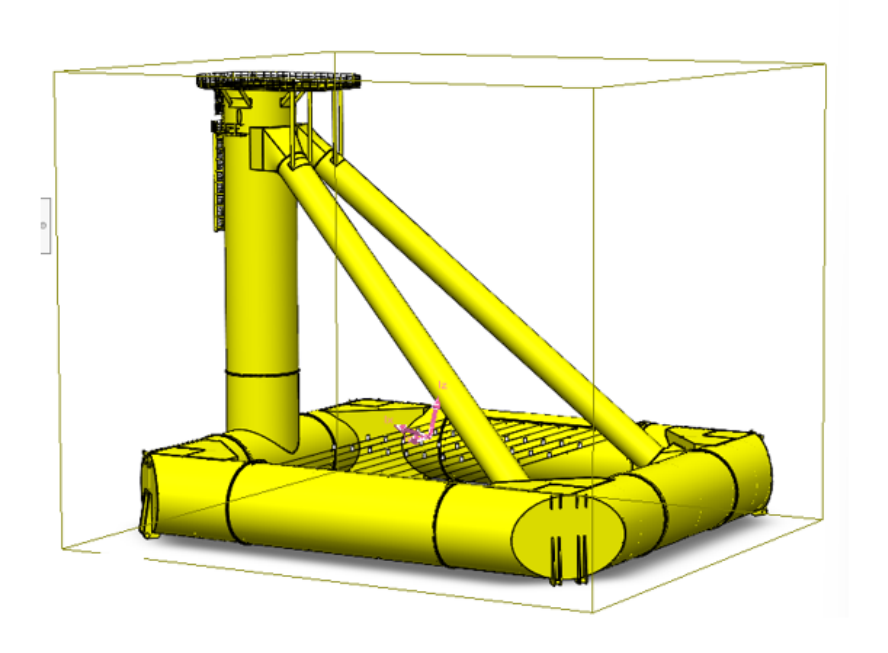


Figure 4.1: Original geometry

satisfy the imposed constraints.

In the SALOME model employed for the optimization, several simplifications have been introduced. Secondary structural details—such as stiffeners, local reinforcements, and minor connection elements—have been neglected, as their influence on global hydrostatic and hydrodynamic behavior is minimal compared to the main geometric features. The focus has therefore been placed on preserving the primary volumetric and mass-distribution characteristics, which govern natural periods, stability, and overall motion response. This approach ensures a good balance between computational efficiency and physical representativeness, making the geometry suitable for parametric studies and optimization.

The discretized mesh used for the hydrodynamic analysis in Nemoh, shown in Figure 4.2, consists of 1574 panels generated from the simplified SALOME geometry. The panel size was constrained between a minimum of 2.5 m and a maximum of 5.0 m, providing a good balance between geometric fidelity and computational efficiency. This ensured that the main hydrodynamic features of the platform were accurately represented without introducing unnecessary refinement.

Within the optimisation framework, four geometric parameters are treated as design variables: the column diameter (D_P) , the draft (Draft), the longitudinal base dimension (L_x) , and the ballast length $(L_{Ballast})$. The transverse base dimension (L_y) is not a free variable; instead, it is tied to L_x through a fixed ratio. Specifically,

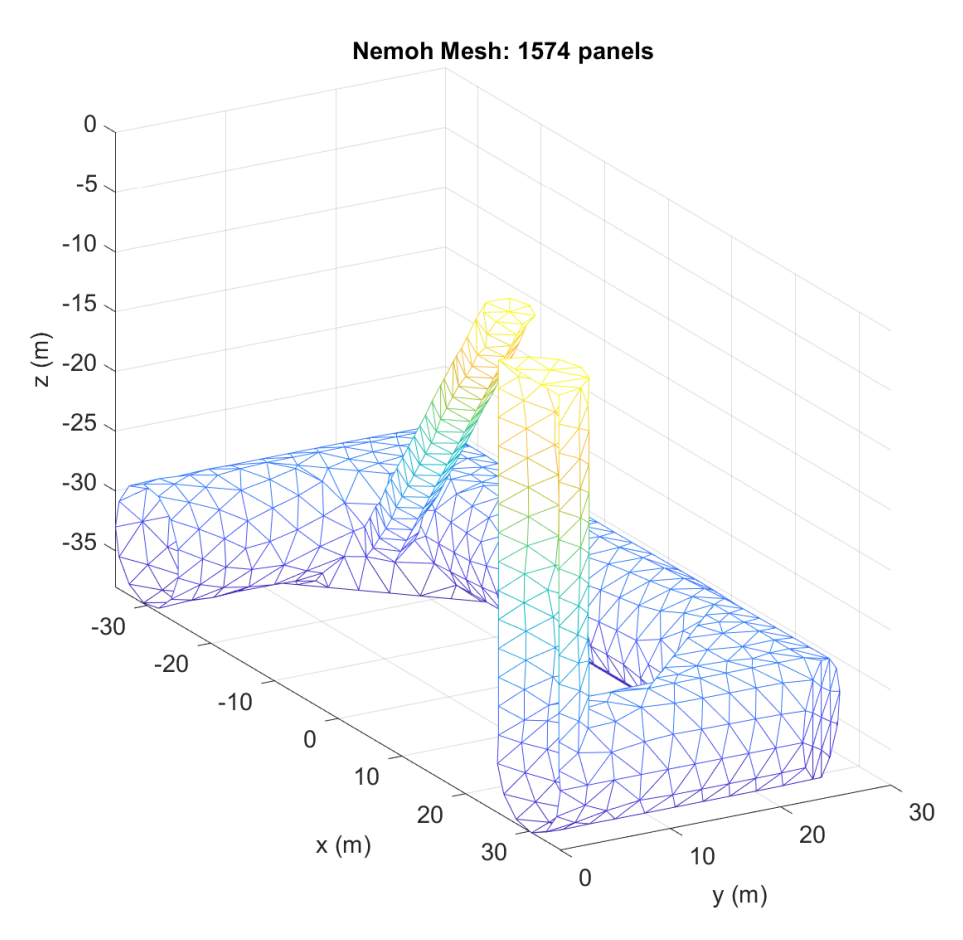


Figure 4.2: Panel mesh of the simplified geometry exported from SALOME and used in Nemoh (1574 panels).

 L_y is scaled proportionally to L_x by adopting the reference aspect ratio, so that the relative proportions of the baseline geometry are preserved while reducing the dimensional design space. Fixing this ratio reduces the design space while preserving a platform close to the reference geometry.

These parameters directly affect hydrostatic and hydrodynamic performance, mass distribution, and platform stability, while all other dimensions (external extensions, pontoon thicknesses, and brace configuration) are kept fixed. Reference values and search ranges are reported in Table 4.1.

Table 4.1: Optimization variables: reference values and search ranges.

Variable	Symbol	Reference value	Range
Pontoon diameter	D_P [m]	10.0	6 - 15
Draft	Draft [m]	38.0	20 - 42
External length (x)	L_x [m]	70.0	45 - 75
Ballast length	$L_{Ballast}$ [m]	5.2	3 - 10

The tendons are modeled as aramid-fiber ropes (Twaron[®]), selected for their high specific stiffness and reduced weight compared to conventional steel tendons. The main mechanical properties (axial stiffness EA, diameter d, minimum breaking load (MBL), and weight per unit length) were interpolated from the manufacturer's datasheet. For each individual in the optimization, tendon diameter and length are updated consistently with the design geometry, ensuring that the mooring system remains physically representative while its influence on stability and cost is captured in the evaluation process.

4.2 Wind Turbine

The reference turbine considered is the IEA 15-MW model developed by the National Renewable Energy Laboratory (NREL). Key parameters are summarised in Table 4.2.

Table 4.2: Key parameters of the IEA 15-MW reference wind turbine [4].

Parameter	Units	Value
Power rating	MW	15
Turbine class	IEC	1B
Rotor diameter	m	240
Hub height	\mathbf{m}	150
Number of blades	-	3
Control	-	Variable speed, collective pitch
Cut-in wind speed	m/s	3
Rated wind speed	m/s	10.59
Cut-out wind speed	m/s	25

Power curves were obtained for wind speeds from cut-in to cut-out, with operating characteristics dictated by the ROSCO controller [2]. These include minimum rotor speed and a maximum allowable thrust, limited to 80% of the maximum as part of the peak-shaving strategy.

For each stiffness and wind speed, steady-state values of rotor speed, blade pitch angle, generator torque, generated power, thrust, and platform pitch angle were determined using an OpenFAST model in the pre-processing phase. The simulation results are used to fit a quadratic polynomial relating AEP to the maximum static pitch angle, providing a computationally efficient formulation within the optimisation process.

Figures 4.3–4.5-4.5 illustrate the precomputed power curves, the resulting AEP values, and the associated steady-state operating conditions at different platform pitch stiffnesses.

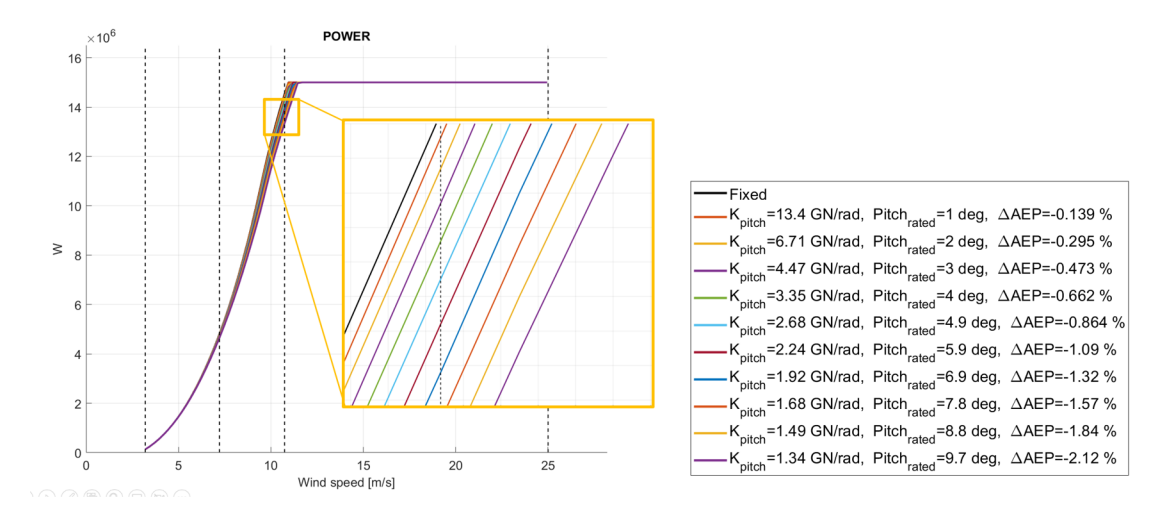


Figure 4.3: Steady-state power curves at different platform pitch stiffnesses.

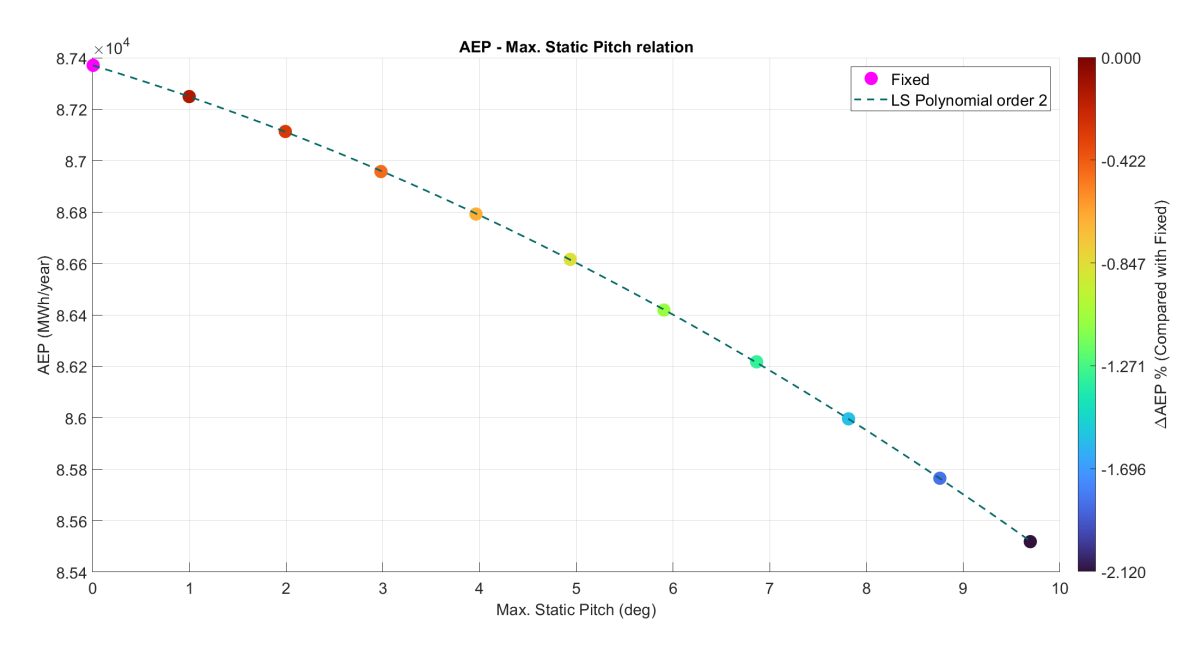


Figure 4.4: AEP at different platform pitch stiffnesses (related to different maximum static pitch angles).

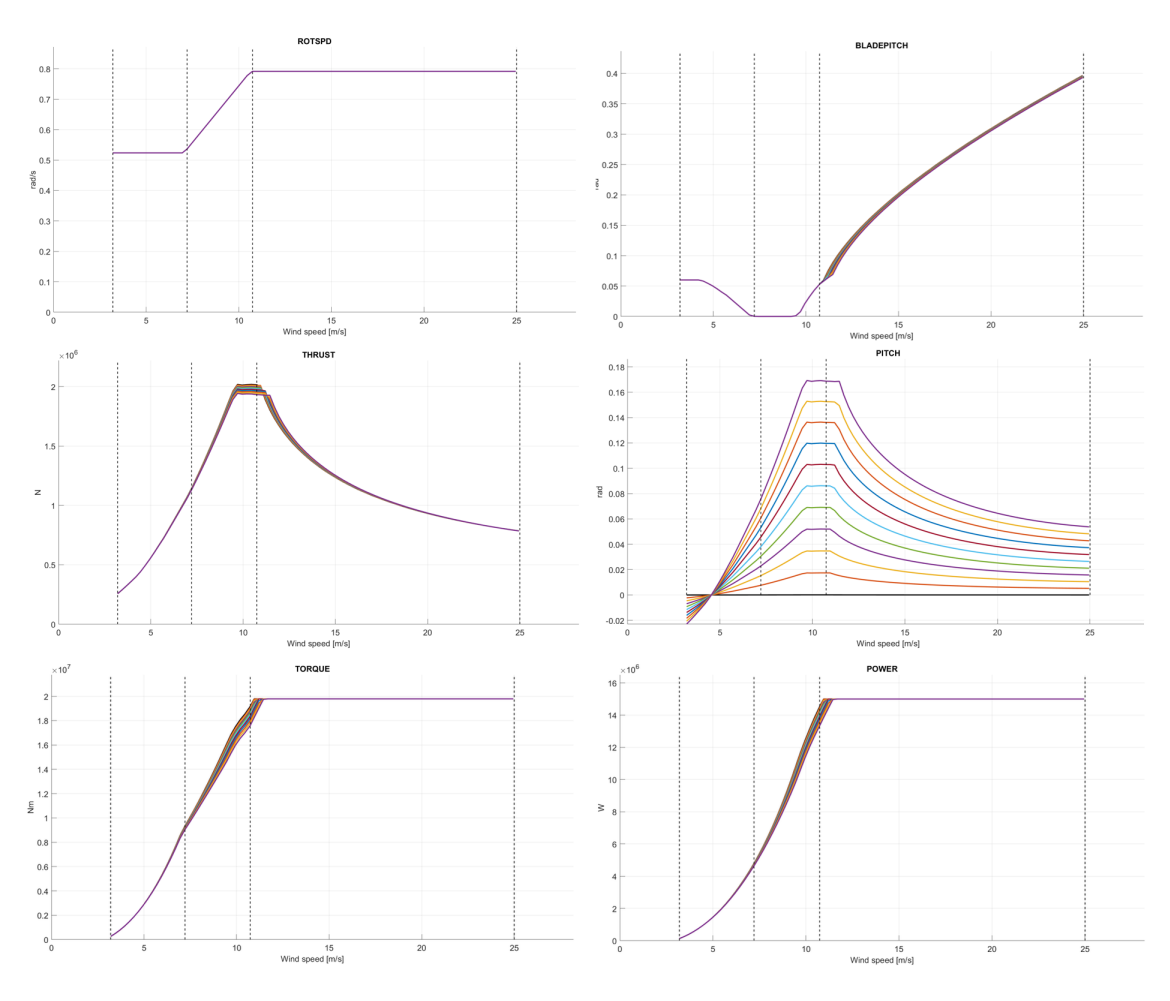


Figure 4.5: Steady-state values of rotor speed, blade pitch angle, generator torque, power, thrust, and structure pitch angle at different platform pitch stiffnesses.

All simulations were performed under simplified conditions, with a constant wind profile, calm sea state (no waves), and additional damping applied such that only the pitch degree of freedom was active. This setup, commonly used in pre-processing studies, isolates the effect of pitch stiffness on turbine behaviour. Each case was simulated long enough to reach steady conditions, after which the output was averaged over a short window to obtain the generator power. In this work, a transient of 500 s followed by a 50 s averaging period are adopted.

Wind speeds were discretised into 0.25 m/s bins (89 values), and eight pitch-stiffness levels were considered (including the fixed configuration), yielding a total of 712 simulations. These precomputed power curves were generated prior to the optimisation and applied consistently across all platform concepts.

4.3 Environmental conditions

The selected site (59.0° N, 2.0° W) is characterized by a water depth of 75 m, an average wind speed of 10.98 m/s, and a distance of approximately 55 km from the nearest port.

The wind resource distribution is reported in Figure 4.6, showing that wind speeds are mostly concentrated between 5 and 15 m/s, with a peak occurrence around 11 m/s. The metocean climate is further described through the joint distribution of significant wave height H_s and peak period T_p (Figure 4.7), which indicates the predominance of moderate sea states, typically with H_s between 1 and 4 m and T_p between 5 and 10 s. Finally, the corresponding JONSWAP spectra are illustrated in Figure 4.8, where the spectral density functions are weighted according to their relative occurrence, highlighting the most representative wave conditions for the site.

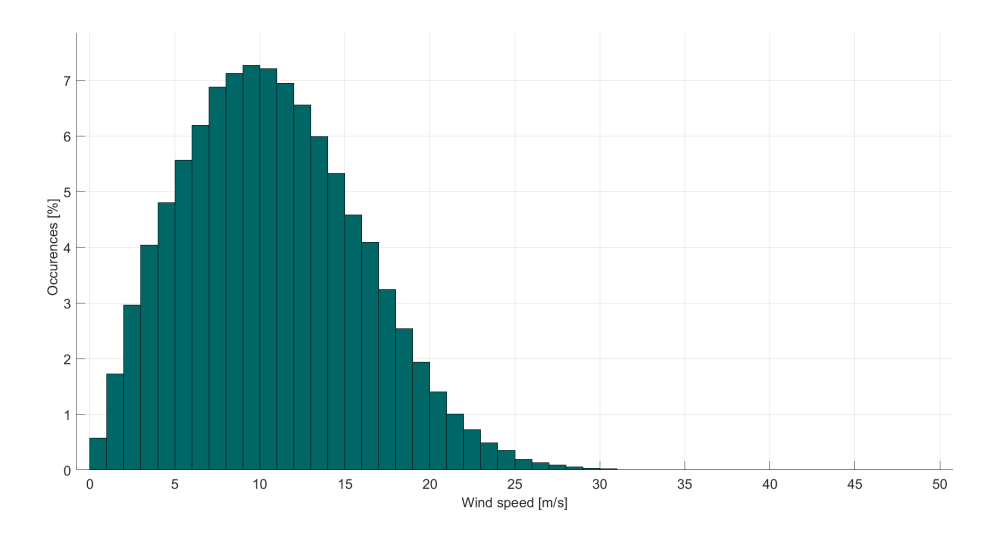


Figure 4.6: Wind speed occurrence distribution.

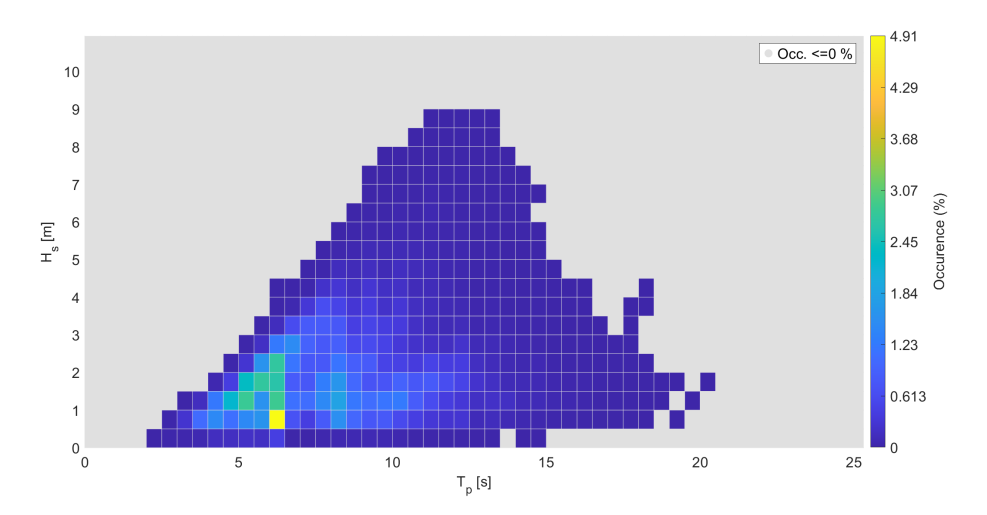


Figure 4.7: Scatter diagram of sea state occurrences in terms of H_s and T_p .

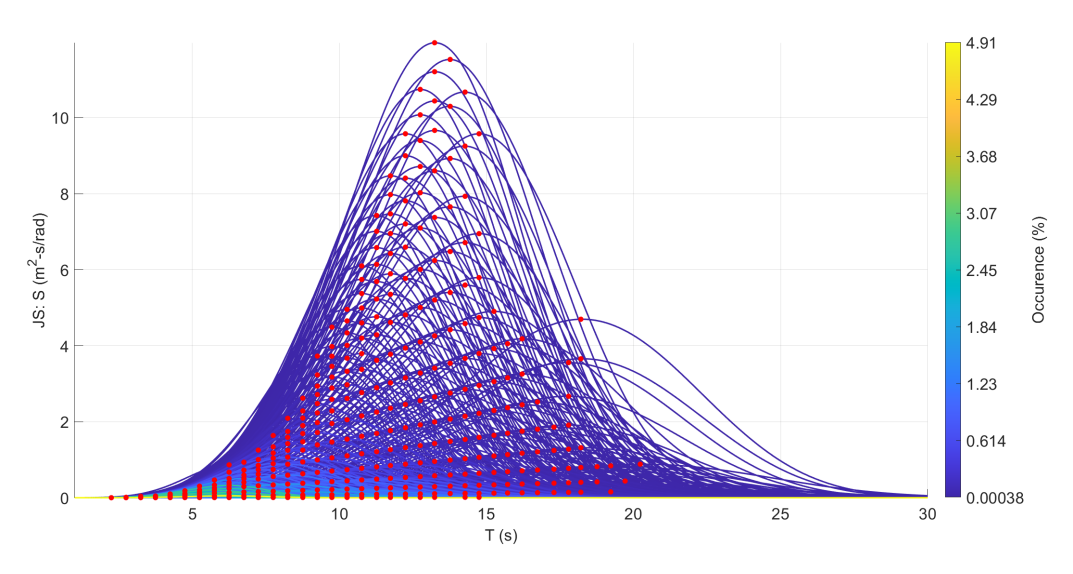


Figure 4.8: Set of JONSWAP spectra weighted by their relative occurrence.

4.4 Optimization framework

4.4.1 Genetic algorithm setup

The NSGA-II algorithm is employed to explore the design space. Regarding the population size and the number of generations, the general rule applied is the following: for problems with fewer than five variables, the population size is set to 50 individuals, while the maximum number of generations is set to $200 \times$ the number of variables. In this thesis, the objective is not to identify the best-performing individual but rather to adapt and validate the optimization framework for the selected case study. For this reason, the setup has been substantially simplified, and the parameters adopted in the trial runs are reported in Table 4.3.

Table 4.3: Main NSGA-II settings.

Option	Value
Crossover fraction	0.66
Pareto fraction	0.70
Population size	20
Max Stall Generation	50
Max Generations	10

4.4.2 Constraints

Constraints are included to guarantee operational reliability. The natural periods are restricted based on site-specific wave spectra (Figure 4.9): surge and sway periods must remain above 20 s, while heave, roll, and pitch periods must remain below 3 s. The static pitch is limited to 7°, and the mooring configuration is restricted to a maximum of two lines per fairlead (eight in total). These constraints guarantee compliance with hydrodynamic and stability requirements within the optimization process.

In consequence of the resonance limits, the frequency window adopted for the hydrodynamic analysis was set between 0.05 and 6.28 rad/s. The discretization included 25 points in the low-frequency range (up to 3 rad/s) and 5 points in the higher-frequency range, in order to adequately resolve the site-specific wave spectrum while limiting computational cost.

Table 4.4: Constraints considered in the optimization.

Constraint	Value / Limit
Surge / Sway resonance period	T > 20 s
Heave / Roll / Pitch resonance period	T < 3 s
Max static pitch angle	7°
Max mooring lines per fairlead	2

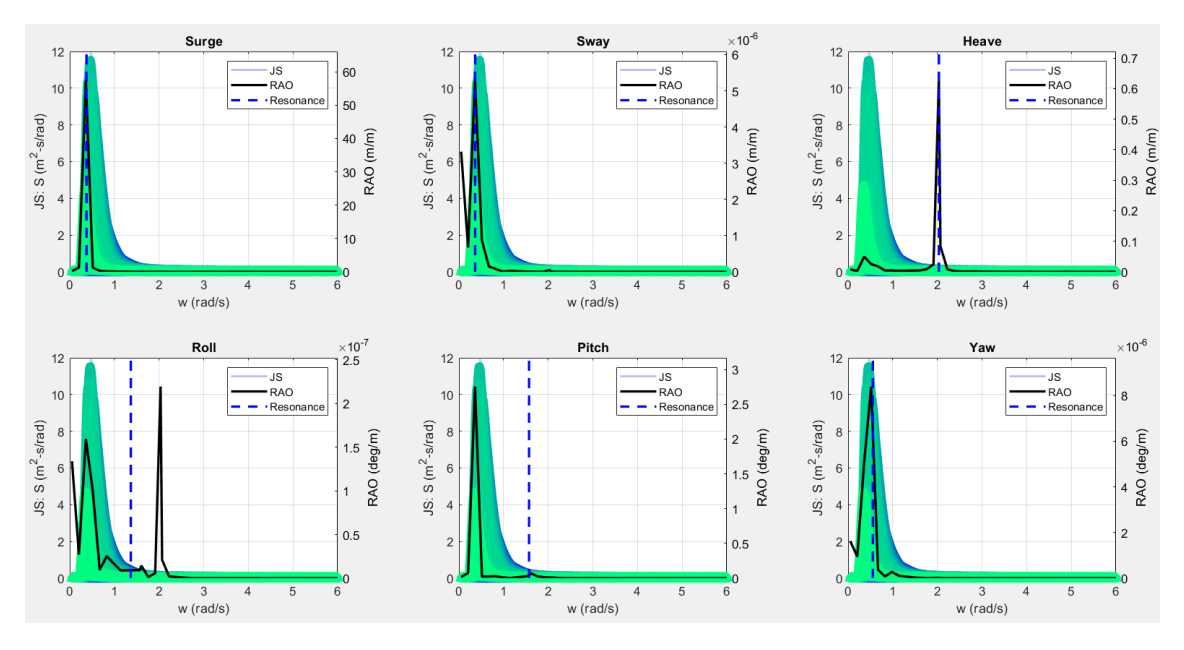


Figure 4.9: RAOs of the reference configuration compared with the site-specific JONSWAP spectrum.

It is important to note that, given the site water depth, the reference configuration of the platform does not satisfy the resonance constraints. As a consequence, the nominal design could not guide the initial population towards feasible solutions, and the optimizer had to search for geometric adjustments to restore compliance with the imposed constraints.

5. Results and Discussions

5.1 Results of techno-economic optimization

The techno-economic optimization simultaneously targets three main objectives:

- Material and manufacturing cost (CAPEX): including steel and mooring lines.
- Annual Energy Production (AEP): evaluated in static conditions by interpolating power curves obtained for different hydrostatic pitch stiffness values.
- Hydrodynamic response (RAO): summarizing the platform's motion response under the site-specific wave climate.

Convergence plots (Figure 5.1) show that the genetic algorithm progressively refined the population across generations. The final distribution of solutions clustered around well-defined Pareto fronts, confirming that the optimizer worked effectively.

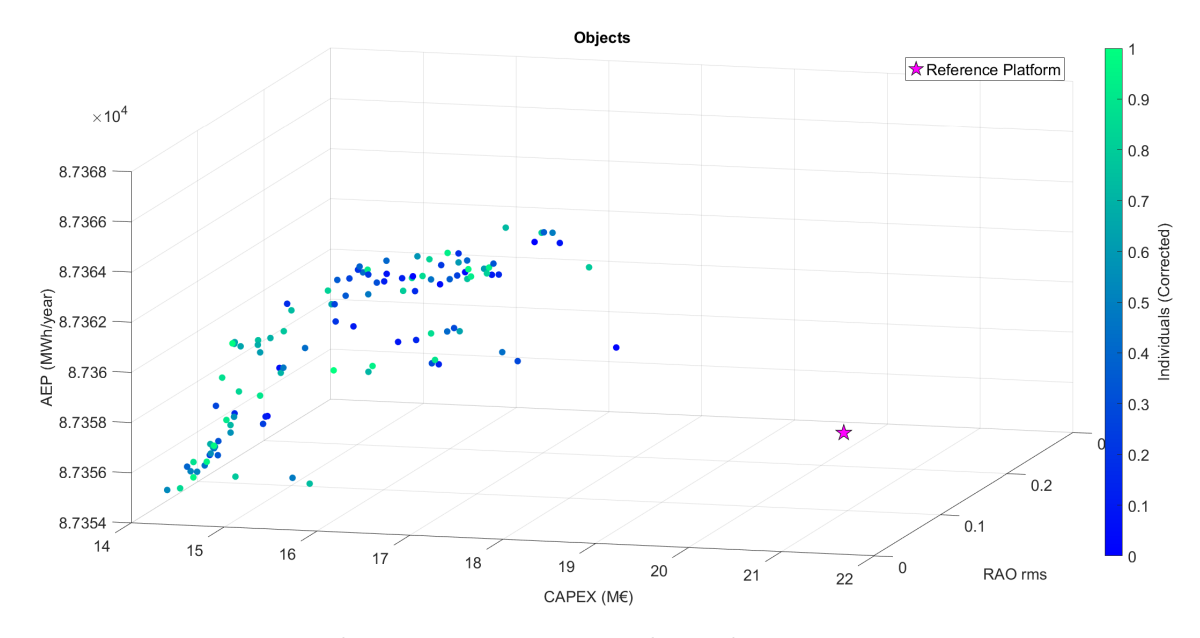


Figure 5.1: Population convergence in the techno-economic optimization.

The main results of the optimisation are illustrated by the Pareto fronts in Figure 5.2–5.3. The normalised front in Figure 5.2 shows that all Pareto-optimal solutions outperform the reference configuration, achieving lower costs and motion amplitudes while maintaining nearly constant energy production. The reference

platform, located well outside the Pareto surface, confirms its limited performance under the selected site conditions.

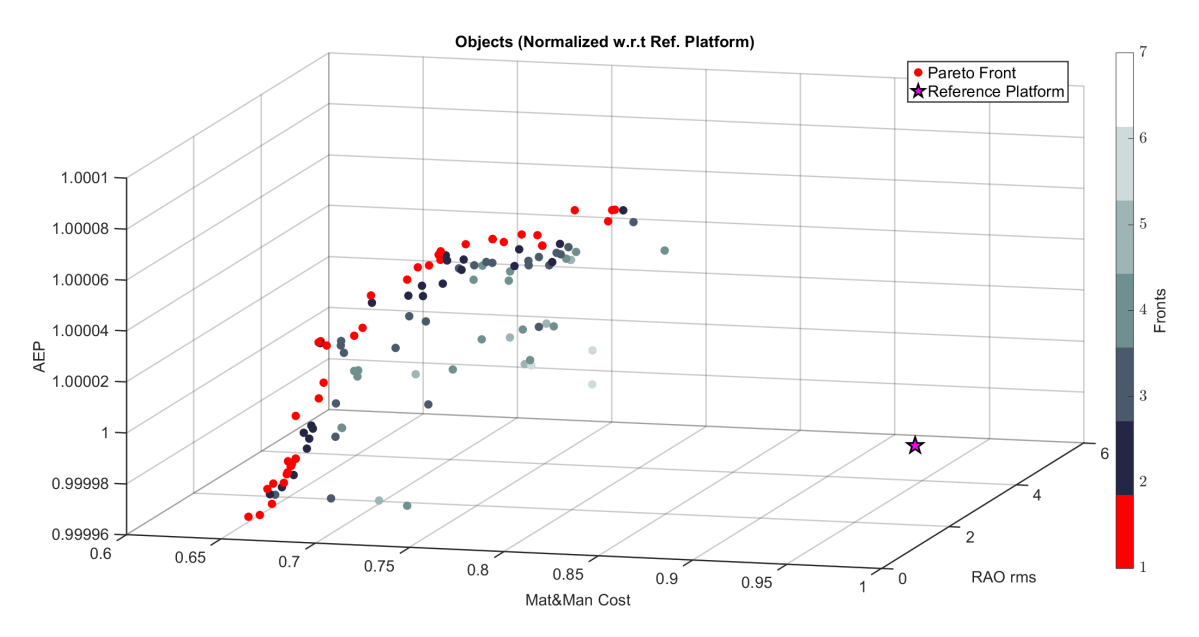


Figure 5.2: Normalised techno-economic Pareto front in the CAPEX–RAO–AEP space with respect to the reference configuration. Values below 1 indicate improvement.

The two-dimensional projections in Figure 5.3 provide a clearer view of the relationships between the objectives. In the cost–RAO plane (bottom panel), the improvement in dynamic stability is particularly evident: a reduction of motion amplitude by a factor of three to four is achieved while simultaneously reducing the manufacturing and material cost by up to 35 %. The cost–AEP and AEP–RAO projections confirm that the annual energy production remains nearly constant across the front, ensuring that dynamic and economic improvements are obtained without penalising energy yield.

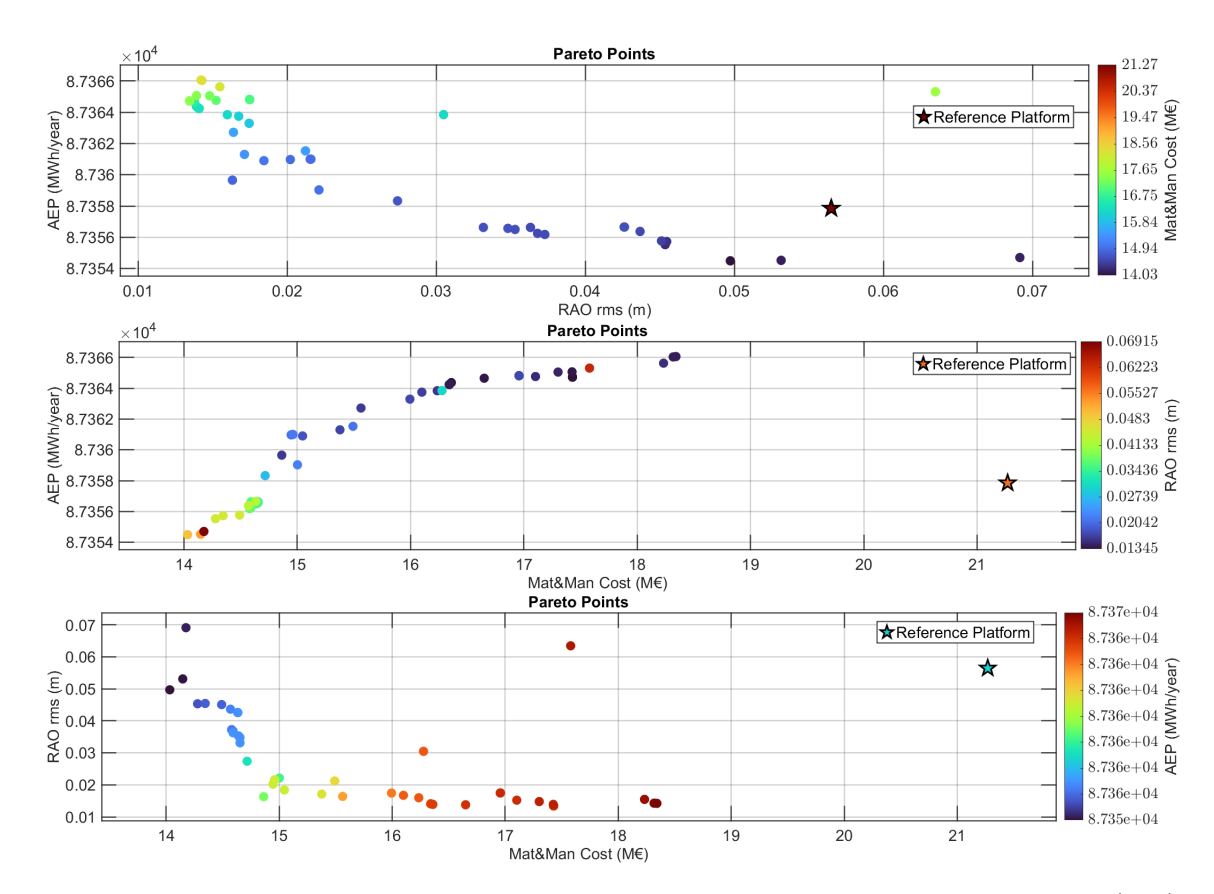


Figure 5.3: Two-dimensional projections of the techno-economic Pareto front: (top) AEP–RAO, (middle) AEP–CAPEX, and (bottom) RAO–CAPEX. The colour scale in each panel represents the third objective.

To better interpret the optimisation trends, Figures 5.4–5.7 show the objectives as a function of the individual design variables. The following observations can be drawn:

- D_P : most feasible designs converged toward smaller diameters (about 6–7 m), which reduced structural mass and cost without compromising hydrodynamic performance.
- Draft: feasible designs span a wide range of draft values, with several efficient solutions found between 28 m and 40 m. Larger drafts generally contribute to improved compliance with the resonance constraint, but no clear monotonic trend is observed. The optimisation balanced stability and cost across different draft levels, indicating that multiple geometric combinations can achieve comparable dynamic performance.
- L_x : the optimisation explored a broad range of values between approximately 45 m and 75 m, without a clear correlation with the objectives. Changes in L_x produced only minor variations in cost and RAO, while AEP remained almost

constant. This indicates that horizontal dimensions have a limited influence on overall performance.

• $L_{Ballast}$: extending the ballast enhanced stability by lowering the centre of gravity and increasing stiffness, complementing the effect of the draft.

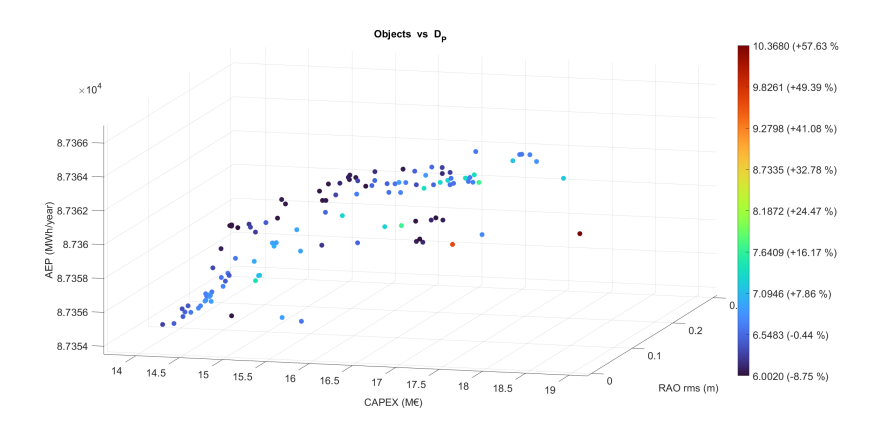


Figure 5.4: Objectives as a function of D_P .

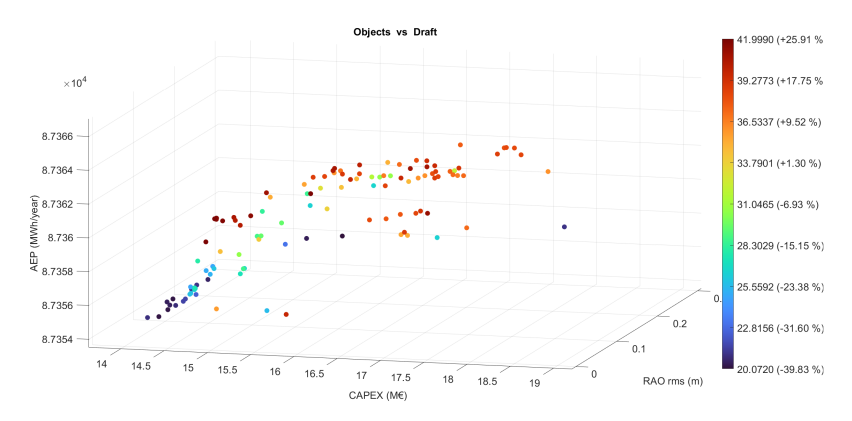


Figure 5.5: Objectives as a function of Draft.

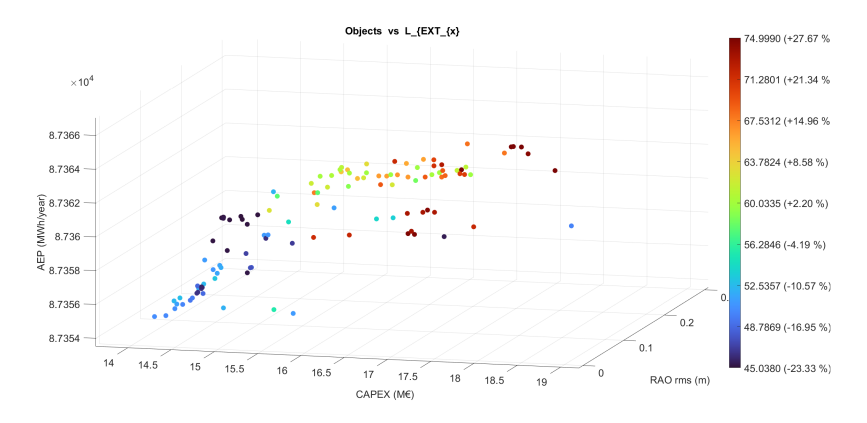


Figure 5.6: Objectives as a function of L_X .

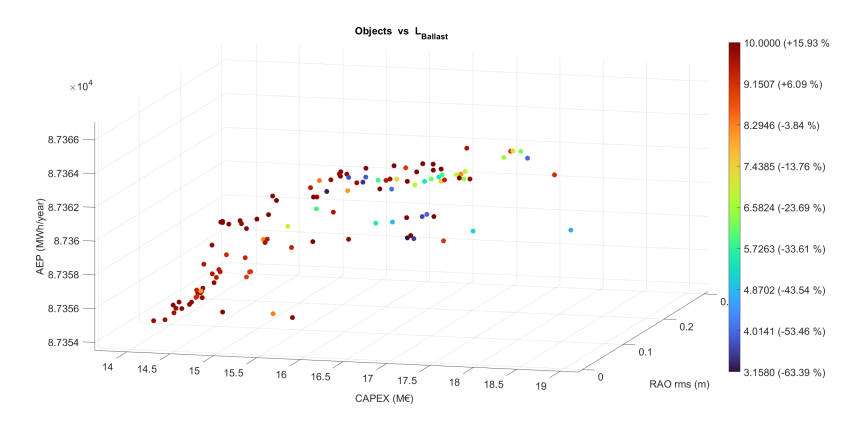


Figure 5.7: Objectives as a function of $L_{Ballast}$.

Overall, the analysis indicates that draft and ballast are the main drivers of hydrodynamic feasibility, while D_P primarily affects cost through its influence on platform mass. Changes in L_x play a secondary role, as most solutions remain close to the reference value. These trends highlight the dependence of the platform's natural periods on its vertical geometry. Variations in draft and ballast length affect the effective mooring line length below the surface, altering the restoring stiffness and, consequently, the dynamic response. This relationship is closely linked to the site water depth: at the considered location, the reference configuration did not meet the resonance constraints due to insufficient separation between structural and wave frequencies.

The influence of the mooring line properties is illustrated in Figure 5.8. Larger line diameters increase material costs but also enhance the restoring stiffness, leading to reduced motion amplitudes. The effect on AEP remains minimal, confirming that the mooring system mainly affects the balance between cost and dynamic response.

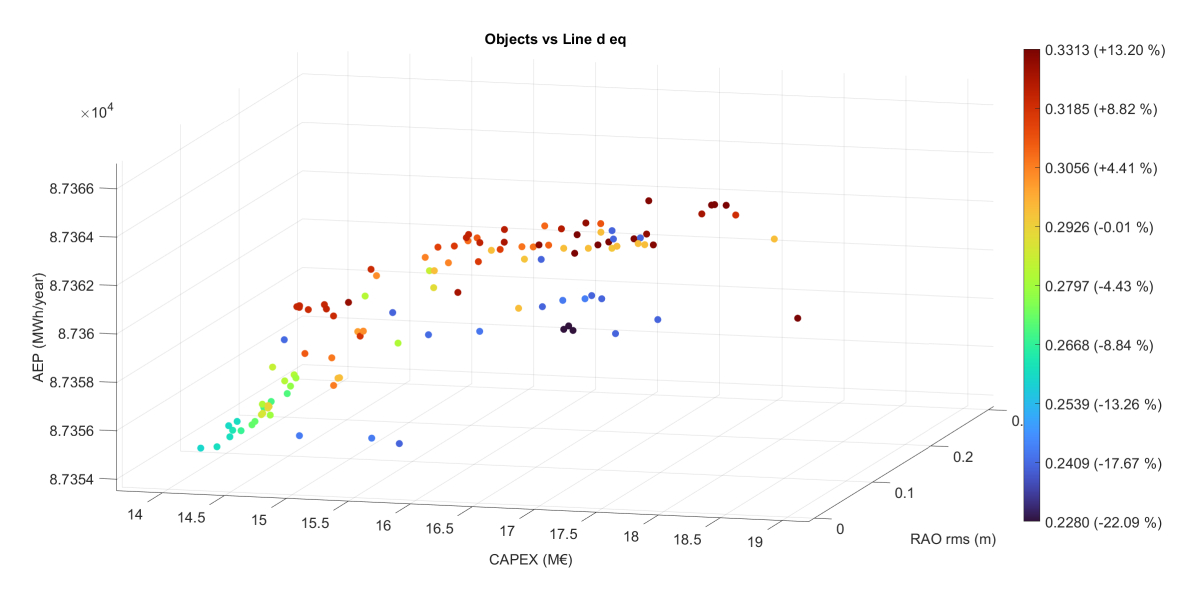


Figure 5.8: Objectives as a function of mooring line equivalent diameter.

5.2 Results of techno-environomic optimization

The techno-environomic optimisation extends the previous framework by introducing the embodied emissions (EOP) as a third objective alongside the cost of power (COP) and the hydrodynamic response (RAO). This formulation enables a combined evaluation of economic efficiency, dynamic behaviour, and environmental impact, providing a more comprehensive view of the platform's sustainability. Although the annual energy production (AEP) is not explicitly included as an objective in this case, it remains implicitly accounted for through the normalisation of both COP and EOP with respect to the energy output, ensuring that designs are still evaluated in terms of their overall performance and productivity.

The optimisation behaviour is broadly similar to the techno-economic case, with the population progressively converging towards a well-defined Pareto front (Figures 5.9–5.10). In the final Pareto distribution, COP and EOP appear nearly collinear, revealing a strong correlation between cost and embodied carbon emissions, while RAO acts as the main discriminating factor across the front. This behaviour arises from the simplified environmental formulation adopted here, in which both COP and EOP scale with the overall structural mass.

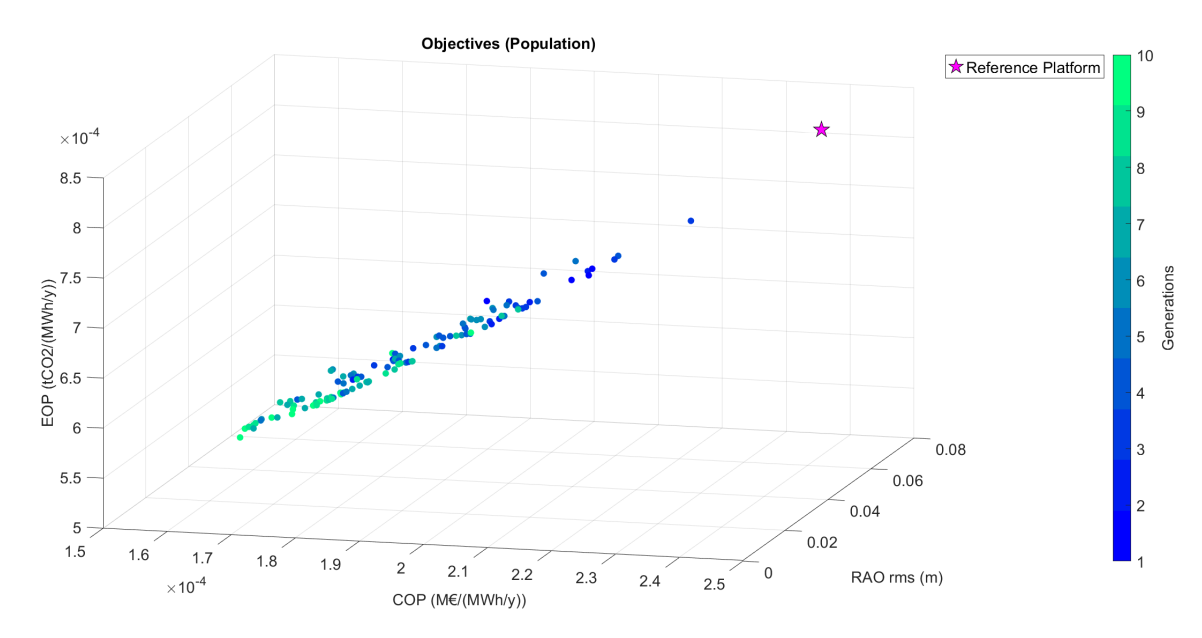


Figure 5.9: Population convergence in the techno-environomic optimization.

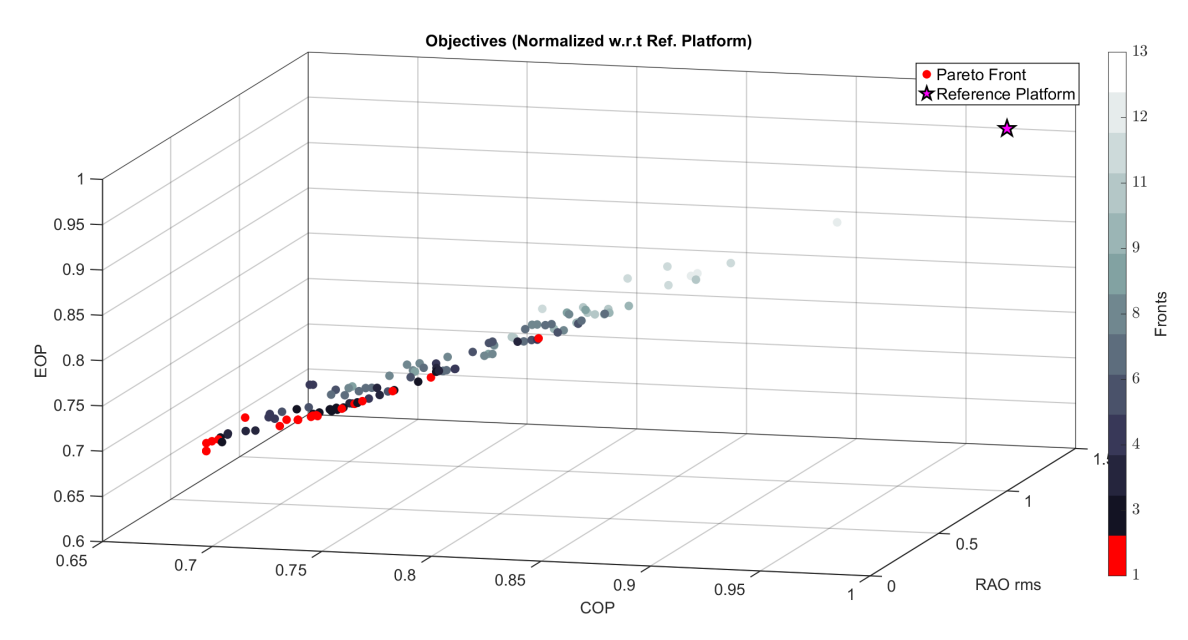


Figure 5.10: Normalised techno-environomic Pareto front in the COP–RAO–EOP space with respect to the reference configuration. Values below 1 indicate improvement.

The two-dimensional projections in Figure 5.11 confirm this coupled trend: in the COP–EOP plane, the nearly linear relationship indicates that reductions in cost correspond almost directly to reductions in embodied emissions. As a result, the optimisation explores a single dominant direction in the objective space, whereas RAO introduces the main trade-off between stability and material intensity. The reference configuration lies well outside the Pareto surface, showing simultaneous improvement in all objectives.

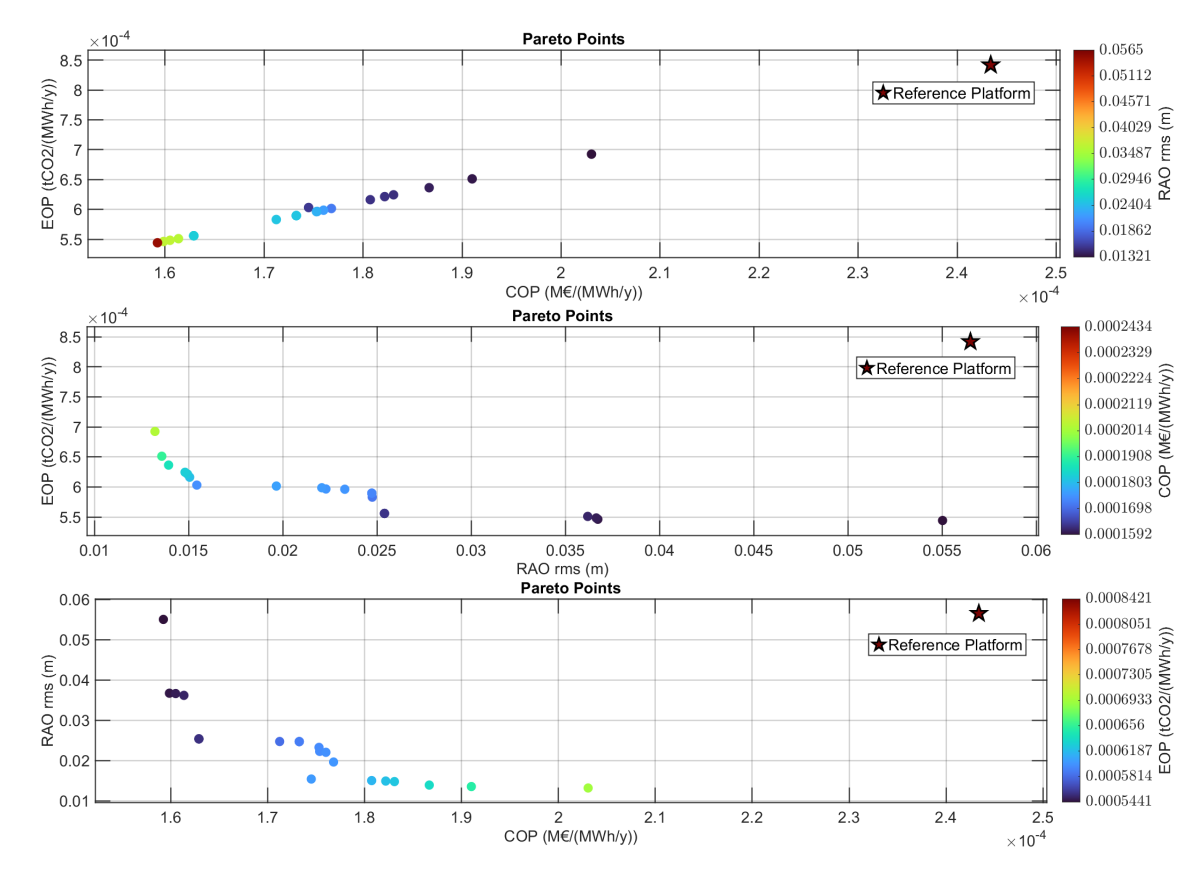


Figure 5.11: Two-dimensional projections of the techno-environomic Pareto front: (top) EOP–COP, (middle) EOP–RAO, and (bottom) RAO–COP. The colour scale in each panel represents the third objective.

The relationships between the design variables and the objectives (Figures 5.12–5.16) follow trends consistent with those observed in the techno-economic case. In both analyses, the pontoon diameter D_P remains the main driver of cost and emissions, as reductions in diameter directly decrease structural mass without significantly affecting stability. Vertical parameters, namely draft and ballast length, continue to govern hydrodynamic behaviour: increasing either parameter generally enhances stability, but in this case it also leads to higher embodied emissions due to greater material use. The horizontal dimension L_x shows only minor influence, confirming its secondary role. Overall, the techno-environomic optimisation reproduces the same physical mechanisms identified previously, with the additional insight that environmental performance closely follows mass-related economic trends.

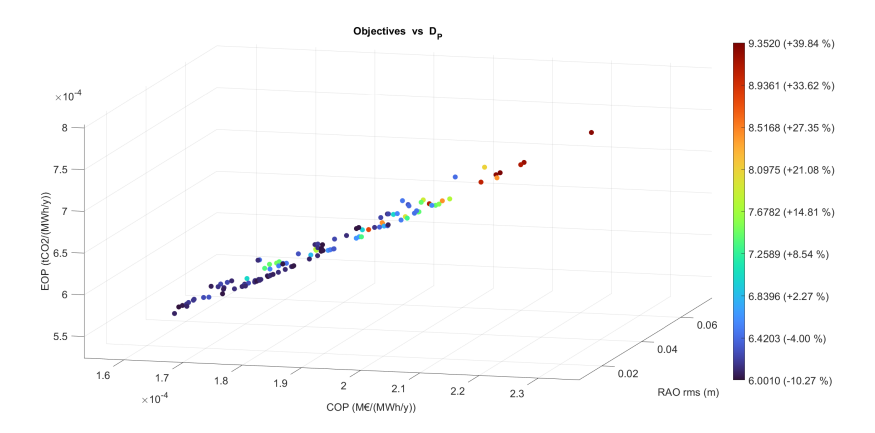


Figure 5.12: Objectives as a function of D_P .

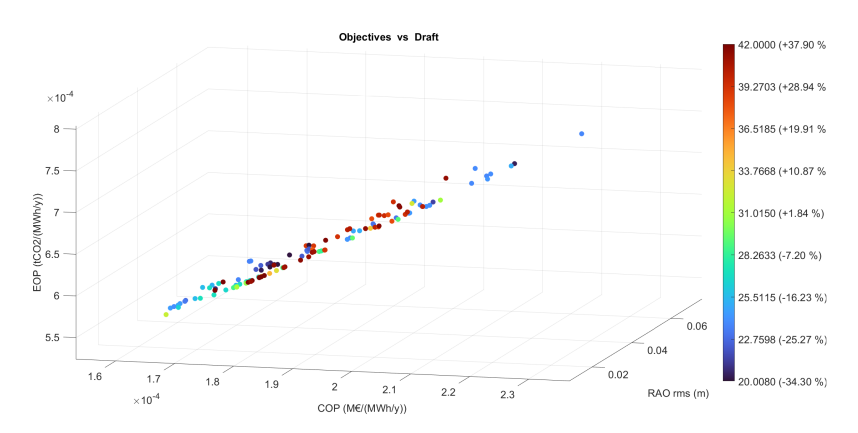


Figure 5.13: Objectives as a function of Draft.

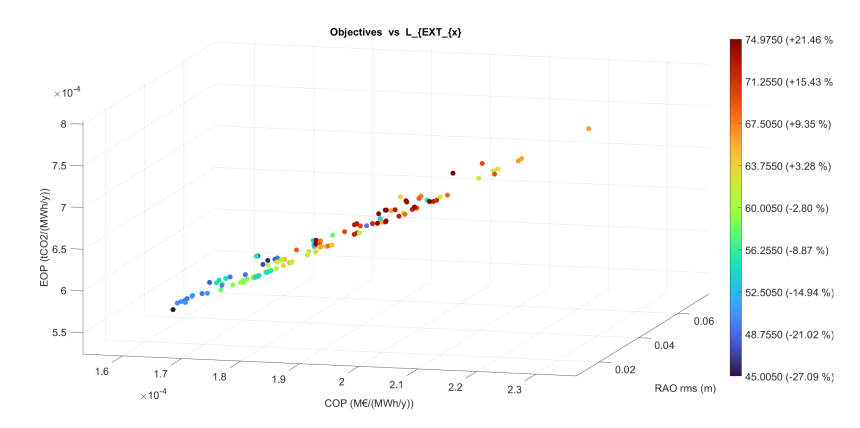


Figure 5.14: Objectives as a function of L_x .

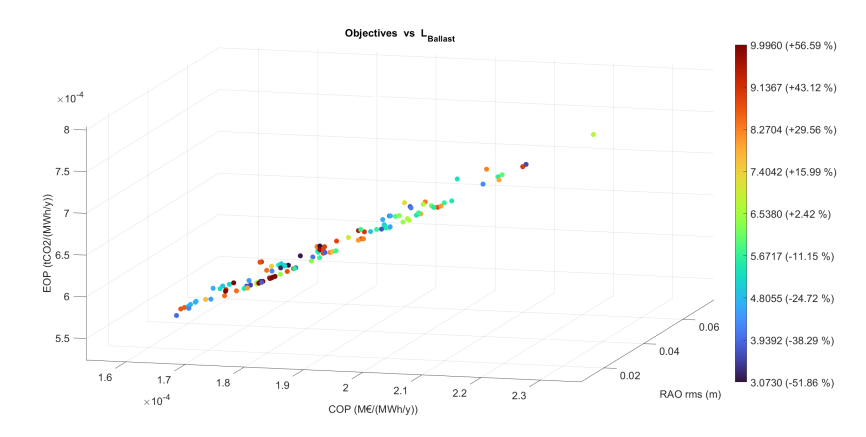


Figure 5.15: Objectives as a function of $L_{Ballast}$.

The effect of the mooring line diameter, shown in Figure 5.16, also mirrors the previous case. Larger lines increase both cost and emissions but contribute to lower RAO values, confirming the presence of a clear techno-environomic trade-off between dynamic stability and environmental impact.

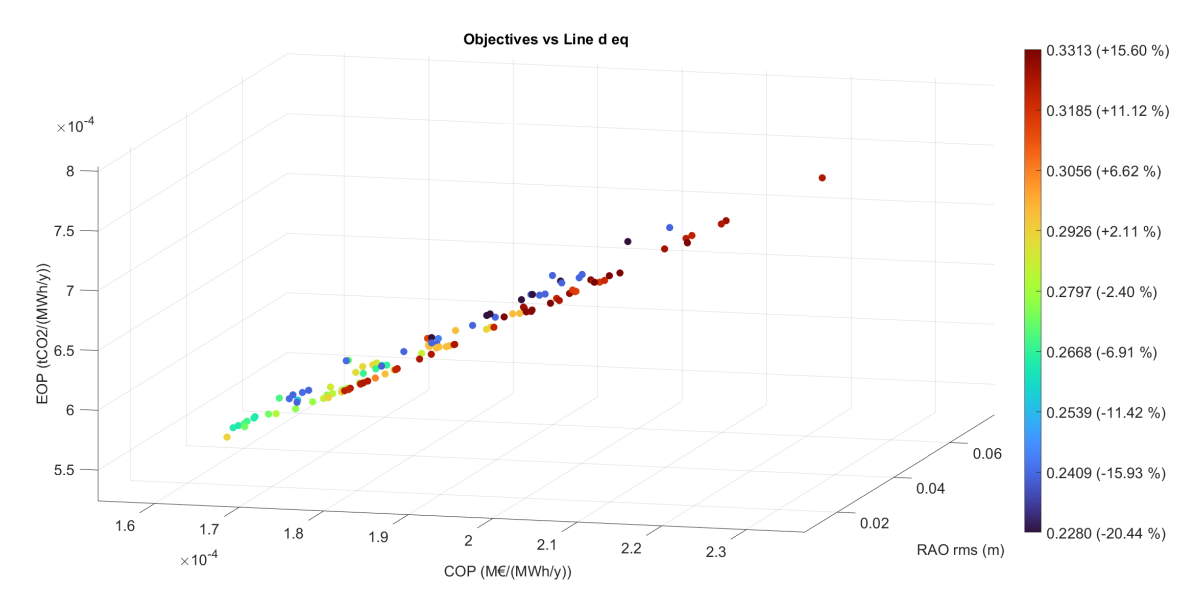


Figure 5.16: Objectives as a function of equivalent mooring line diameter.

Overall, the inclusion of the environmental objective confirms the strong link between cost and embodied emissions, both mainly driven by structural mass. Although the optimisation did not yet yield an independent environmental trade-off, it highlights consistent trends between economic and environmental performance, which will be further examined in the analysis of the selected individuals and in the general discussion.

5.3 Selected individuals

The analysis then proceeds with the selection of candidate designs from the Pareto front. Before performing this selection, a post–processing step was introduced to filter the obtained population. After removing infeasible individuals (constraint violations and divergent objectives) a local Pareto front was obtained and used as the basis for the representative selection.

The selection itself can be carried out from two perspectives:

- phenotype-based, privileging uniformity in the objective space (performance indicators),
- genotype-based, privileging diversity in the design space (decision variables and constructability).

In this study, the latter approach was adopted. The genotype clustering procedure allowed to retain a set of representative designs distributed across the feasible design space, thus capturing a broader range of geometric configurations while keeping their performance within the most relevant window of the Pareto front. This choice was motivated by the main objective of the analysis, which is not to identify a single optimal solution, but rather to explore the relationship between geometry and performance across different trade-offs. By ensuring geometric diversity, the selected individuals provide a clearer picture of how variations in draft, ballast, pontoon diameter, and platform length influence the platform's dynamic, economic, and environmental behaviour.

Techno-economic optimisation

Figure 5.17 shows the techno-economic Pareto front in the CAPEX–RAO–AEP space, with the selected individuals highlighted. As already stated, the inverse relationship between cost and hydrodynamic response is evident: configurations with higher stiffness and lower motion amplitudes are generally associated with larger drafts and longer ballast sections, which increase hydrostatic restoring forces but also add mass and cost. Despite these differences, all designs achieve nearly constant energy production, confirming that the trade-off primarily occurs between cost and dynamic stability.

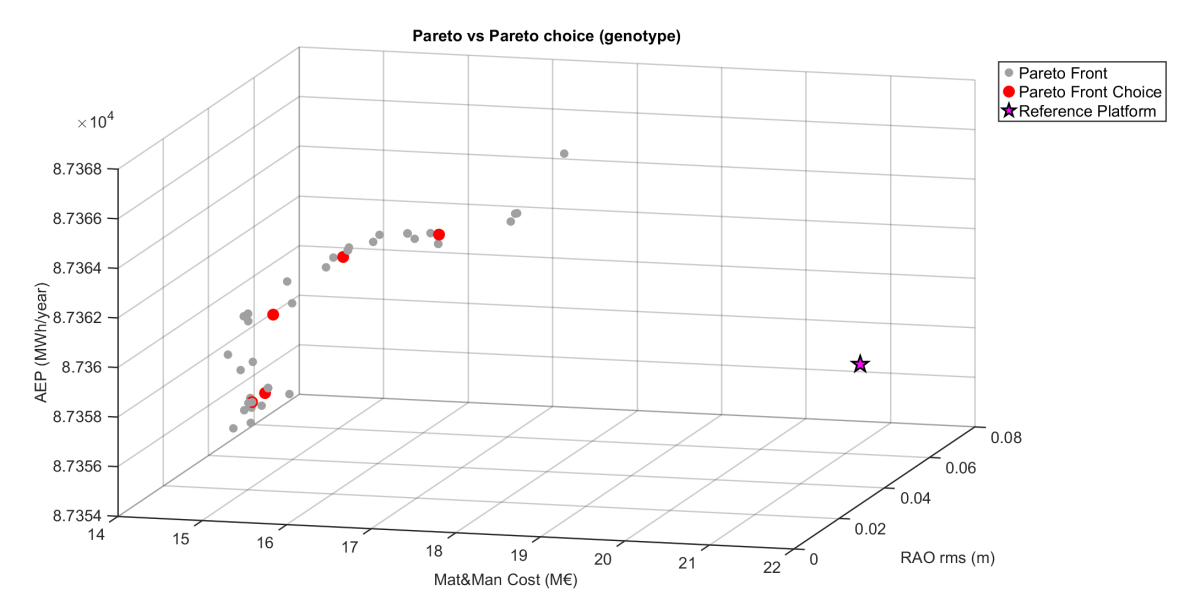


Figure 5.17: Techno-economic Pareto front with genotype-based selected individuals (red) and reference configuration (black).

The radar plots in Figure 5.18 illustrate the geometric variability within the Pareto set. Moderate adjustments of draft (ranging from 21 to 42 m) and ballast length (around 9–10 m) account for most of the variation in stability, while the pontoon diameter converges around 6–7 m, about 30% smaller than the reference (10 m). These changes modify buoyancy and stiffness sufficiently to reduce motion response by a factor of three to four with only moderate cost penalties.

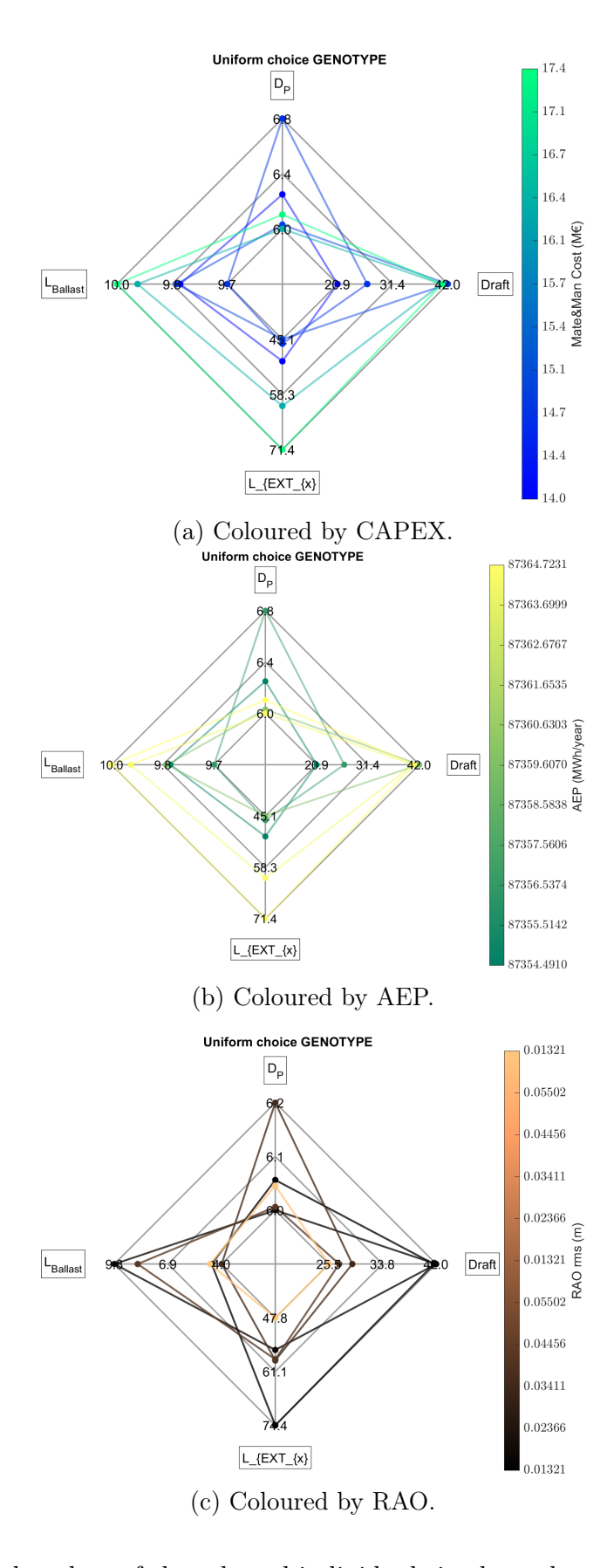


Figure 5.18: Radar plots of the selected individuals in the techno-economic optimisation.

Table 5.1: Selected individuals from the techno-economic optimisation and reference configuration.

Ind.	D_P	Draft	L_{EXT_x}	$L_{Ballast}$	CAPEX	RAO	AEP
	[m]	[m]	[m]	[m]	[M€]	[-]	[GWh/y]
Ref.	10.00	38.00	70.00	5.20	21.27	0.056	87.36
1	6.15	40.89	71.37	9.99	17.43	0.0135	87.37
2	6.29	20.91	50.37	9.81	14.03	0.0497	87.35
3	6.08	41.98	45.15	9.82	14.86	0.0163	87.36
4	6.05	40.77	61.01	9.93	16.36	0.0139	87.36
5	6.83	26.58	46.21	9.68	14.65	0.0348	87.36

Compared with the reference configuration, all designs achieve lower costs (20–35%) and markedly smaller motion amplitudes. Individuals 1 and 4 reach the highest stability, with RAO values about one quarter of the reference, while Individuals 2 and 5 represent lighter and less stable but more economical variants. Individual 3 provides an intermediate balance between the two extremes. Overall, the selected configurations capture the narrow trade-off space where small geometric variations produce measurable shifts in stiffness and cost efficiency.

Techno-environomic optimisation

The techno-environomic optimisation introduces embodied emissions (EOP) as an additional objective alongside the cost of power (COP) and RAO. Figure 5.19 shows the corresponding Pareto front, where the selected designs, highlighted in red, again represent a diverse sampling of feasible geometries.

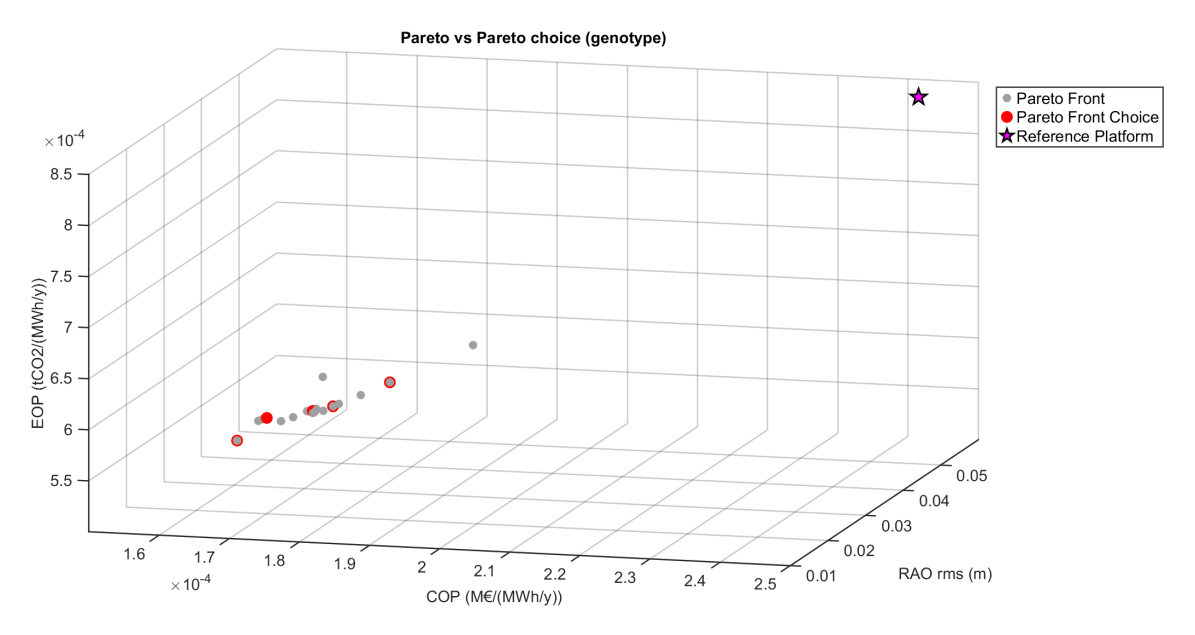


Figure 5.19: Techno-environomic Pareto front with genotype-based selected individuals (red) and reference configuration (black).

The selected designs, detailed in Table 5.2, achieve COP values between 0.16 and 0.20 M€/GWh·y and EOP levels between 540 and 690 tCO₂/GWh·y, compared with 0.24 M€/GWh·y and 842 tCO₂/GWh·y for the reference. RAO values decrease to 0.013–0.025, corresponding to roughly a fourfold improvement in dynamic stability. Most designs maintain pontoon diameters close to 6 m, confirming its strong influence on both cost and emissions. Differences arise mainly from vertical adjustments: deeper drafts and longer ballast sections (up to 42 m and 9.8 m) improve stability but increase embodied emissions due to added steel mass.

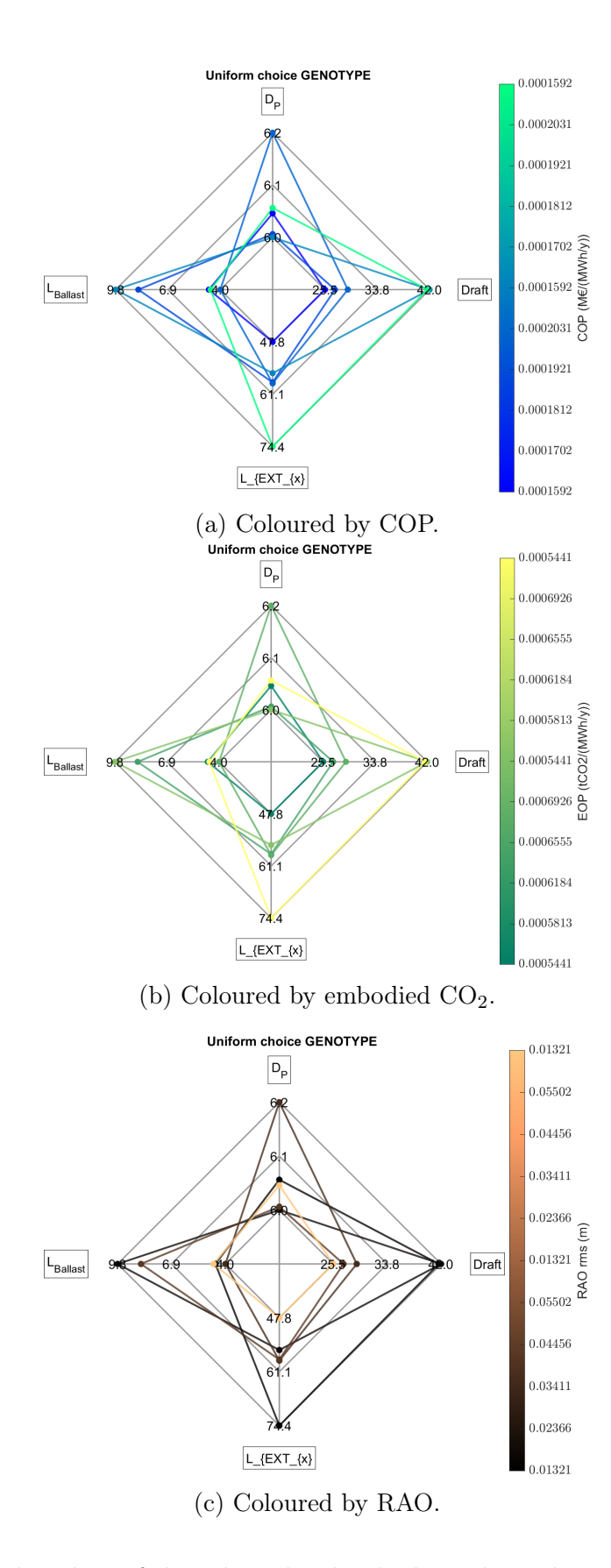


Figure 5.20: Radar plots of the selected individuals in the techno-environomic optimisation.

Table 5.2: Selected individuals from the techno-environomic optimisation and reference configuration.

Ind.	D_P	Draft	L_{EXT_x}	$L_{Ballast}$	COP	RAO	EOP
	[m]	[m]	[m]	[m]	$\left[\frac{M\mathfrak{C}}{GWh\cdot y}\right]$	[-]	$\left[\frac{\mathrm{tCO}}{\mathrm{GWh \cdot y}}\right]$
Ref.	10.00	38.00	70.00	5.20	0.243	0.0565	842
1	6.06	25.53	47.76	4.63	0.159	0.0550	544
2	6.01	42.00	55.71	9.75	0.182	0.0149	621
3	6.20	29.12	58.31	4.00	0.176	0.0221	599
4	6.02	27.10	58.05	8.51	0.171	0.0247	583
5	6.07	41.66	74.36	4.54	0.203	0.0132	693

All optimised configurations outperform the reference in both cost and emissions, achieving simultaneous reductions of 15–35%. The differences among individuals mainly reflect how each balances material efficiency and stability: lighter geometries minimise cost and emissions but exhibit higher motion amplitudes, whereas deeper and stiffer designs achieve lower RAO at modest environmental penalties. These results confirm that multiple geometric pathways can lead to comparable technoenvironmental performance, forming a continuum of feasible trade-offs rather than a single optimal solution.

5.4 General discussion

The two optimisation exercises highlight how geometric parameters simultaneously influence the dynamic, economic, and environmental performance of the platform. Although based on simplified formulations, both cases show consistent and physically coherent trends, demonstrating that the developed framework can capture the main trade-offs among cost, stability, and mass efficiency.

In both analyses, the nominal configuration proved dynamically unsuitable for the site, failing the resonance constraint due to insufficient hydrostatic stiffness. The optimiser compensated for this limitation by adjusting the vertical geometry and restoring feasibility. This outcome confirms the strong dependence of natural periods on vertical proportions and mooring stiffness, as well as the capability of the workflow to autonomously adapt geometry to site-specific hydrodynamic conditions.

In the techno-economic case, the total capital cost of the Pareto-optimal solutions spans approximately 14–17 M€, while the motion response amplitude decreases from about 0.05 for the lightest configurations to nearly 0.013 for the most stable ones.

The annual energy production remains almost constant at around 87 GWh·y⁻¹, confirming that improvements in stability and cost efficiency can be achieved without penalising power output. Overall, the Pareto front reveals a clear inverse correlation between cost and motion response: lighter and cheaper platforms exhibit larger motions, whereas deeper and heavier ones achieve improved stiffness at a moderate cost increase.

The techno-environomic optimisation reproduces the same physically consistent tendencies observed in the techno-economic case, confirming the internal coherence of the framework. The total capital cost of the Pareto-optimal solutions lies between 15 and 16 M \in , with the cost of power ranging from 0.16 to 0.20 M \in -GWh⁻¹ and embodied emissions from approximately 540 to 700 tCO₂·GWh⁻¹. Because both cost and emissions are primarily governed by the structural steel mass, the two indicators remain strongly correlated, and the inclusion of the environmental objective does not yet produce a distinct diversification of the Pareto front. Instead, it reinforces the same design tendencies—favouring light, stiff, and mass-efficient configurations—while coherently extending the analysis to include embodied impacts.

From a geometric perspective, the techno-environomic solutions converge towards drafts between 25 and 42 m, external lengths between 48 and 74 m, and ballast extensions from 4 to 10 m, while maintaining pontoon diameters around 6 m. Compared with the techno-economic case, these designs slightly reduce both the overall length and the ballast size, thereby lowering the total structural mass. This behaviour reflects the influence of the environmental objective, which promotes massefficient geometries that minimise embodied emissions while maintaining sufficient draft to ensure hydrodynamic stiffness and compliance with resonance constraints. Physically, the resulting configurations achieve a delicate balance between buoyancy, stiffness, and material efficiency, demonstrating that multiple lightweight geometries can reach comparable techno-environmental performance within the feasible design space.

The obtained objective values are consistent with the typical orders of magnitude reported for floating offshore wind platforms of comparable scale, although they tend to fall on the lower side of the expected range. This outcome is reasonable, as the present work adopts several simplifying assumptions and excludes certain cost components such as anchoring, installation, and maintenance logistics. Consequently, the results should be regarded as preliminary indicators of relative performance rather than absolute predictions. The comparison indicates that both optimisation exercises converge towards a common design philosophy: platforms that are lightweight yet sufficiently stiff to ensure dynamic stability. Rather than converging

to a single optimum, the results outline a continuum of feasible configurations, each representing a distinct compromise between cost, stiffness, and environmental impact. Such insight is particularly valuable during the early design phase, where the objective is to understand the sensitivity of performance to geometric adjustments rather than to define precise dimensions. The selected individuals discussed in the previous sections further illustrate this behaviour. Despite differences in draft and ballast proportions, their performance remains comparable, indicating that similar objectives can be achieved through alternative geometric combinations. This consistency confirms that the optimiser identifies physically meaningful trade-offs instead of isolated numerical minima, providing a robust foundation for the comparative discussion and subsequent conclusions.

While the framework successfully reproduces coherent and physically meaningful trends, it deliberately relies on several simplifications introduced to maintain computational efficiency while preserving the essential physics of the problem. The hydrodynamic analysis was performed in the linear frequency domain, neglecting viscous effects, non-linear excitation, and turbine–platform coupling. As a consequence, the computed RAO values should be interpreted as reliable indicators of relative stability, whereas detailed time-domain analyses will be required to obtain absolute motion predictions for the selected configurations. Similarly, the annual energy production was estimated from static interpolation of precomputed power curves, an approach that captures first-order geometric effects and enables rapid comparison across hundreds of designs, while refined dynamic simulations can later be applied to the most promising individuals to quantify absolute AEP values.

The techno-economic and environmental formulations also reflect an initial balance between model simplicity and scope. By focusing on the dominant steel and mooring contributions, the framework captures the main mass-driven relationships among objectives, while keeping the analysis computationally tractable. These assumptions provide a solid starting point for future developments, where more detailed cost breakdowns, installation processes, and life-cycle inventories will be progressively incorporated to achieve a comprehensive, quantitative optimisation of floating wind platforms.

Overall, the trends emerging from both optimisation exercises confirm that the methodology captures the key physical relationships linking geometry, cost, stability, and embodied impacts. The developed workflow thus provides a coherent foundation for future extensions within the INF⁴INiTY project, supporting the transition from an exploratory design tool to a fully integrated decision-support system for sustainable floating wind development.

6. Conclusions

This thesis presented a multi-objective optimisation framework for the preliminary design of the GICON-SOF tension-leg platform supporting the IEA 15 MW reference wind turbine, developed within the INF⁴INiTY project. The methodology integrates hydrodynamic, techno-economic and environmental elements into a single workflow, offering a robust approach for assessing floating offshore wind substructures across different performance domains.

The framework combines parametric geometry generation in SALOME, hydrodynamic analysis in NEMOH, and simplified techno-economic and environmental models, coupled through the NSGA-II genetic algorithm. By varying the main geometric parameters (e.g. pontoon diameter, draft, external length and ballast extension) the optimisation study investigates how changes in geometry affect the platform's stability, cost and environmental impact, while satisfying hydrostatic and mooring constraints. To explore these interactions from complementary perspectives, two optimisation studies were carried out: a techno-economic one, focused on the balance between cost and dynamic behaviour, and a techno-environomic one, which extends the techno-economic analysis to include embodied carbon emissions. Both exercises produced consistent and physically meaningful results:

- In the techno-economic case, the optimiser identified configurations achieving up to 35% lower capital cost and a fourfold improvement in hydrodynamic stability compared with the reference design, without reducing energy production. Draft and ballast length proved to be the main factors influencing stability, while the pontoon diameter primarily affected cost.
- In the techno-environomic case, the inclusion of the embodied carbon emissions indicator confirmed a strong correlation between cost and carbon footprint, both mainly driven by structural mass. The optimisation still produced lighter, more efficient and more stable designs, with 15–35% lower cost and emissions than the baseline design. In addition, the optimal design based on the techno-environomic framework also resulted in a more stable platform, reducing RAO values by a factor of three to four. Although cost and carbon emissions objectives remain partially coupled, the results highlight clear trends toward lighter and more material-efficient geometries.

The proposed framework proved to be robust and adaptable. Starting from a reference configuration that did not satisfy the imposed constraints, the algorithm consistently converged toward mass-efficient and dynamically stable solutions, showing its ability to adapt the platform geometry to site-specific conditions. The chosen modelling strategy enabled the efficient evaluation of many design alternatives while retaining the key physical mechanisms governing platform performance.

To keep the optimisation computationally efficient, some simplifying assumptions were introduced. The hydrodynamic analysis was performed in the linear frequency domain, neglecting viscous damping, non-linear wave excitation, and the coupling between platform motion and turbine control. The annual energy production was estimated using static interpolation of precomputed power curves as a function of pitch stiffness, capturing the main geometric effects but excluding dynamic control behaviour. Finally, the cost and carbon emissions models considered only the dominant steel and mooring contributions, excluding anchors, installation and end-of-life phases. For this reason, the results should be interpreted as relative indicators useful for identifying trends and comparing designs, rather than as absolute predictions.

Outlook

Future work should focus on extending the framework toward a more comprehensive and quantitative design tool. Possible developments include:

- Adding anchors, installation, operation and end-of-life processes to the cost and emission models, in order to separate economic and environmental objectives more clearly;
- Coupling with time-domain simulations and turbine-control models to perform detailed dynamic analyses of the selected individuals, improving the accuracy of RAO-based stability indicators and AEP estimates by capturing the full aero-hydro-servo dynamics;
- Incorporating the optimisation of Nature-Inclusive Design (NID) features, assessing their influence on both cost and embodied carbon emissions while promoting ecological co-benefits and site-specific environmental compatibility;
- Extending the optimisation to multi-platform and farm-scale problems, considering array layout and inter-turbine interactions.

Final remarks

Overall, this work provides a coherent foundation for the multi-objective optimisation of floating offshore wind platforms. The results show that targeted geometric modifications can substantially improve both cost efficiency and stability, while the environmental extension introduces a broader and more sustainable design perspective. With further refinement and integration of detailed cost and life-cycle data, the framework can evolve into a complete decision-support tool capable of identifying cost-effective, low-carbon and dynamically stable floating wind concepts, supporting the competitiveness and sustainability of offshore renewable energy.

Bibliography

- [1] Guide to offshore wind foundations: Challenges and opportunities in designing and developing offshore wind foundations both now and in the future. Technical report, Empire Engineering, 2021. Accessed: 2025-09-14.
- [2] Nikhar J. Abbas, Daniel S. Zalkind, Lucy Y. Pao, and Alan D. Wright. A reference open-source controller for fixed and floating offshore wind turbines. Wind Energy Science, 7(1):53–73, 2022.
- [3] Mohammed Khair Al-Solihat and Meyer Nahon. Stiffness of slack and taut moorings. Ships and Offshore Structures, 2015.
- [4] Christopher Allen, Anthony Viselli, Habib Dagher, Andrew Goupee, Evan Gaertner, Nikhar Abbas, Matthew Hall, and Garrett Barter. Definition of the umaine volturnus-s reference platform developed for the iea wind 15-megawatt offshore reference wind turbine. Technical Report NREL/TP-5000-76773, National Renewable Energy Laboratory, 2020.
- [5] Mohammad Barooni, Turaj Ashuri, Deniz Velioglu Sogut, Stephen Wood, and Shiva Ghaderpour Taleghani. Floating offshore wind turbines: Current status and future prospects. *Energies*, 16(1):2, 2023.
- [6] Tony Burton, David Sharpe, Nick Jenkins, and Ervin Bossanyi. Wind Energy Handbook. John Wiley & Sons, Chichester, UK, 2nd edition, 2011.
- [7] Jieyan Chen and Moo-Hyun Kim. Review of recent offshore wind turbine research and optimization methodologies in their design. *Journal of Marine Science and Engineering*, 9(7):1–38, 2021.
- [8] W. E. Cummins. The impulse response function and ship motions. Technical Report Report 1661, David Taylor Model Basin, Department of the Navy, Washington, D.C., 1962.
- [9] Kalyanmoy Deb, Amrit Pratap, Sameer Agarwal, and T. Meyarivan. A fast and elitist multiobjective genetic algorithm: NSGA-II. *IEEE Transactions on Evolutionary Computation*, 6(2):182–197, 2002.
- [10] Lene Eliassen, Jasna B. Jakobsen, Andreas Knauer, and Finn Gunnar Nielsen. Cascade analysis of a floating wind turbine rotor. In *Journal of Physics: Conference Series*, volume 555, page 012053. IOP Publishing, 2014.

- [11] Carlos Ferreira, Antonio Gómez, M. Dolores Esteban, and Deborah Greaves. A holistic tool to assess the cost and performance of floating offshore wind farms. *Renewable Energy*, 102:139–153, 2016.
- [12] Kostas Florios, George Mavrotas, and Danae Diakoulaki. Solving multiobjective, multiconstraint knapsack problems using mathematical programming and evolutionary algorithms. *European Journal of Operational Research*, 203(1):14–21, May 2010.
- [13] Global Wind Energy Council. Global wind report 2025. Technical report, Global Wind Energy Council (GWEC), 2025.
- [14] Matthew Hall, Brad Buckham, and Curran Crawford. Evolving offshore wind: A genetic algorithm-based support structure optimization framework for floating wind turbines. In *Proceedings of the 32nd International Conference on Ocean, Offshore and Arctic Engineering (OMAE 2013)*, Nantes, France, 2013. ASME.
- [15] Klaus Hasselmann, Tim P. Barnett, Ed Bouws, Hans Carlson, D. E. Cartwright, K. Enke, J. A. Ewing, Hans Gienapp, D. E. Hasselmann, Peter Kruseman, Arend Meerburg, Peter Müller, Dirk J. Olbers, Klaus Richter, Werner Sell, and Hans Walden. Measurements of wind-wave growth and swell decay during the joint north sea wave project (jonswap). Ergaenzungsheft zur Deutschen Hydrographischen Zeitschrift, Reihe A, 1973.
- [16] Meysam Karimi, Matthew Hall, Brad Buckham, and Curran Crawford. A multi-objective design optimization approach for floating offshore wind turbine support structures. *Journal of Ocean Engineering and Marine Energy*, 3:69–87, 2017.
- [17] Michael Kausche, Frank Adam, Frank Dahlhaus, and Jochen Großmann. Floating offshore wind economic and ecological challenges of a tlp solution. Renewable Energy, 126:270–280, 2018.
- [18] Jacob Ladenburg. Stated public preferences for on-land and offshore wind power generation—a review. Wind Energy, 12(2):171–181, 2009.
- [19] Mareike Leimeister, Athanasios Kolios, and Maurizio Collu. Development of a framework for wind turbine design and optimization. *Modelling*, 2(1):105–128, 2021.
- [20] Anders Myhr, Catho Bjerkseter, Anders Ágotnes, and Tor Anders Nygaard. Levelised cost of energy for offshore floating wind turbines in a life cycle perspective. Renewable Energy, 66:714–728, 2014.

- [21] Francesco Papi and Alessandro Bianchini. Technical challenges in floating offshore wind turbine upscaling: A critical analysis based on the nrel 5 mw and iea 15 mw reference turbines. Renewable and Sustainable Energy Reviews, 162:112489, 2022.
- [22] Katarzyna Patryniak, Maurizio Collu, and Andrea Coraddu. Multidisciplinary design analysis and optimisation frameworks for floating offshore wind turbines: State of the art. *Ocean Engineering*, 251:111002, 2022.
- [23] Willard J. Pierson Jr and Lionel Moskowitz. A proposed spectral form for fully developed wind seas based on the similarity theory of sa kitaigorodskii. *Journal of Geophysical Research*, 69(24):5181–5190, 1964.
- [24] Hanne Lerche Raadal, Bjørn Ivar Vold, Anders Myhr, and Tor Anders Nygaard. Ghg emissions and energy performance of offshore wind power. Renewable Energy, 66:614–622, 2014.
- [25] Rasul Satymov, Dmitrii Bogdanov, and Christian Breyer. Techno-economics of offshore wind power in global resolution. *Applied Energy*, 393:125980, 2025.
- [26] Tyler Stehly, Patrick Duffy, and Daniel Mulas Hernando. Cost of wind energy review: 2024 edition. Technical Report NREL/TP-5000-91775, National Renewable Energy Laboratory, Golden, CO, USA, November 2024.
- [27] George Struthers, Stuart Gill, Rohan A. Kishore, Chris White, and Henry Jeffrey. Life cycle assessment of four floating offshore wind farms around scotland. Energies, 16(15):5669, 2023.
- [28] Victoria Sykes, Maurizio Collu, and Andrea Coraddu. A review and analysis of optimisation techniques applied to floating offshore wind platforms. *Ocean Engineering*, 285:115247, 2023.
- [29] Victoria Sykes, Maurizio Collu, and Andrea Coraddu. A review and analysis of the uncertainty within cost models for floating offshore wind farms. Renewable and Sustainable Energy Reviews, 186:113634, 2023.
- [30] Chenggong Tan and Xiaorong Sun. Review on advancements and challenges of offshore floating wind turbine platforms. *International Journal of Frontiers in Engineering Technology*, 7(2):108–117, 2025.
- [31] WindEurope. Wind energy in europe: 2024 statistics and the outlook for 2025-2030. Technical report, WindEurope, February 2025.

[32] Bowen Zhou, Zhibo Zhang, Guangdi Li, Dongsheng Yang, and Matilde Santos. Review of key technologies for offshore floating wind power generation. *Energies*, 14(24):8144, 2021.